Jets in pp collisions in the ALICE Experiment

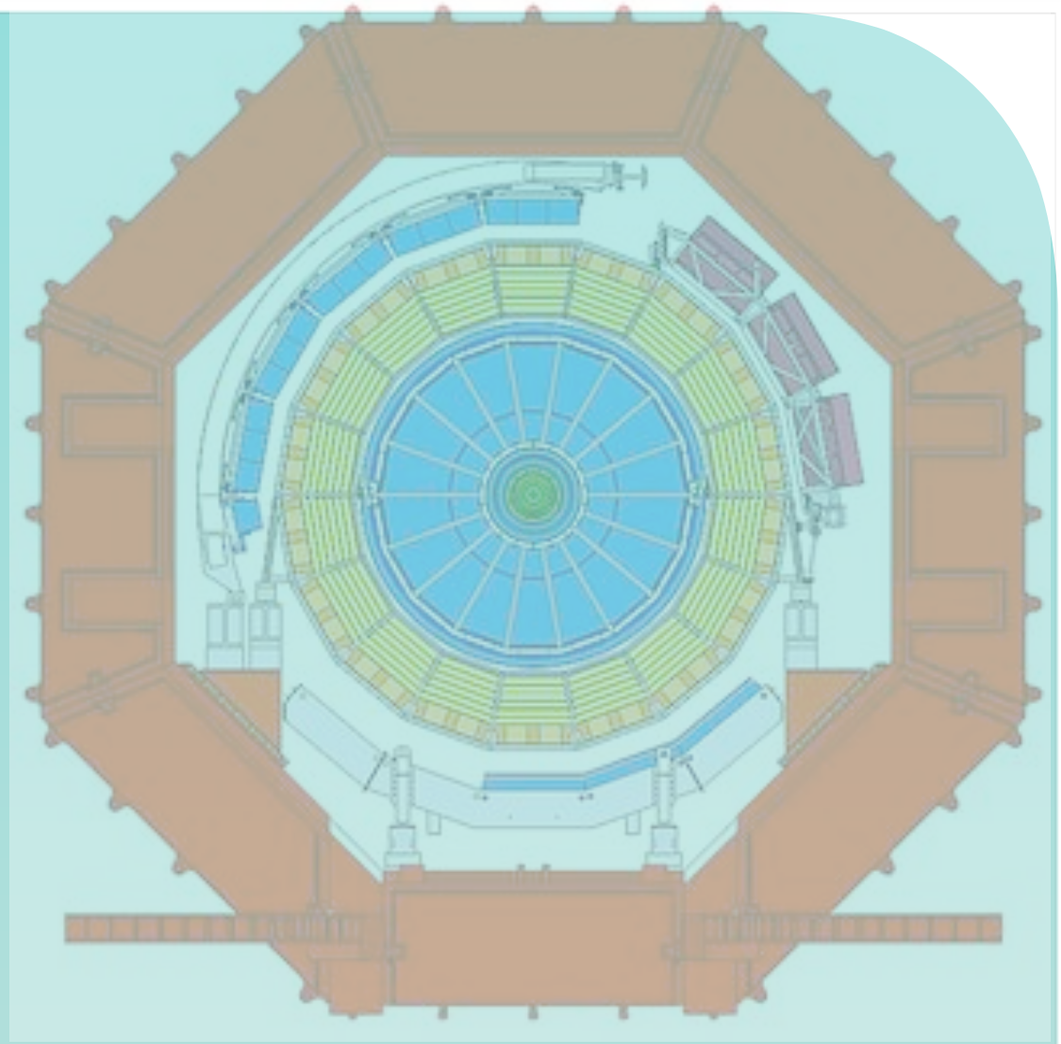

Debjani Banerjee,
UIUC

Hot Jet Workshop
Jan 08 - 10, 2025

UNIVERSITY OF ILLINOIS URBANA-CHAMPAIGN

Importance of jet study: pp collisions

What is jet?

Theory: Jets are cascade of partons produced from fragmentation of hard scattered quarks/ gluons in the initial stage of collision

Experiment: Collimated showers of final state particles resulting from fragmentation of hard scattered partons in high-energy collisions

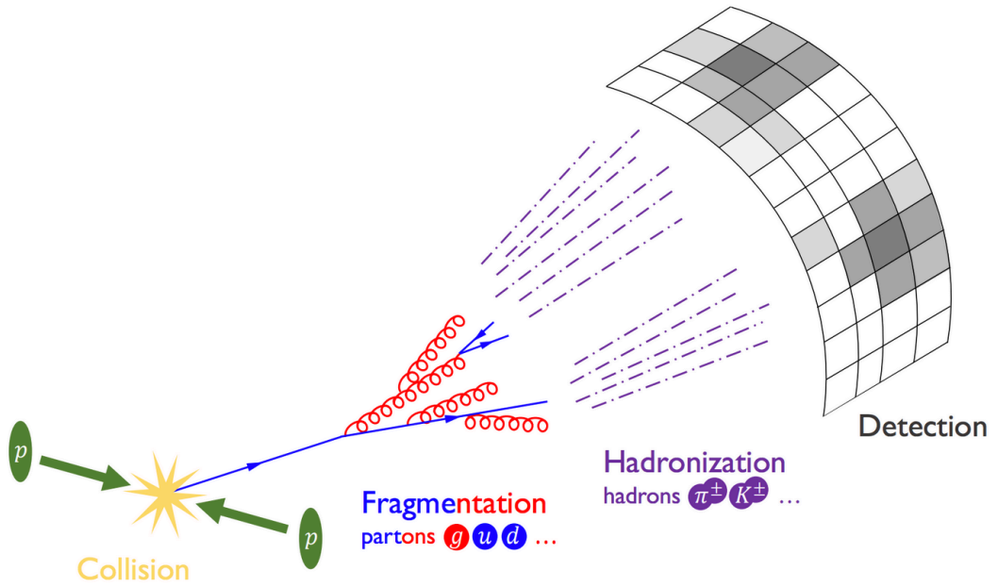

Jets in proton-proton (pp) collisions [1]

[1] https://www.ericmetodiev.com/post/jetformation/

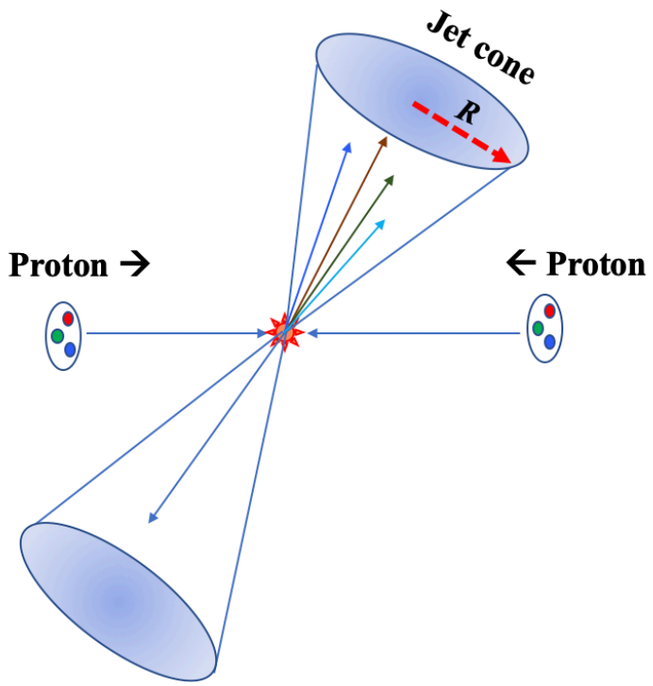

Jet study in pp collisions

- Jet measurements in pp collisions serve as a baseline for similar measurements in heavy-ion collisions
- Jet production in pp collisions enables to test pQCD calculations
- Measurements of jet production and its properties are used to tune different Monte Carlo event generator

Importance of jet study: High Multiplicity pp collisions

QGP-like signatures in pp collisions!

Strangeness enhancement

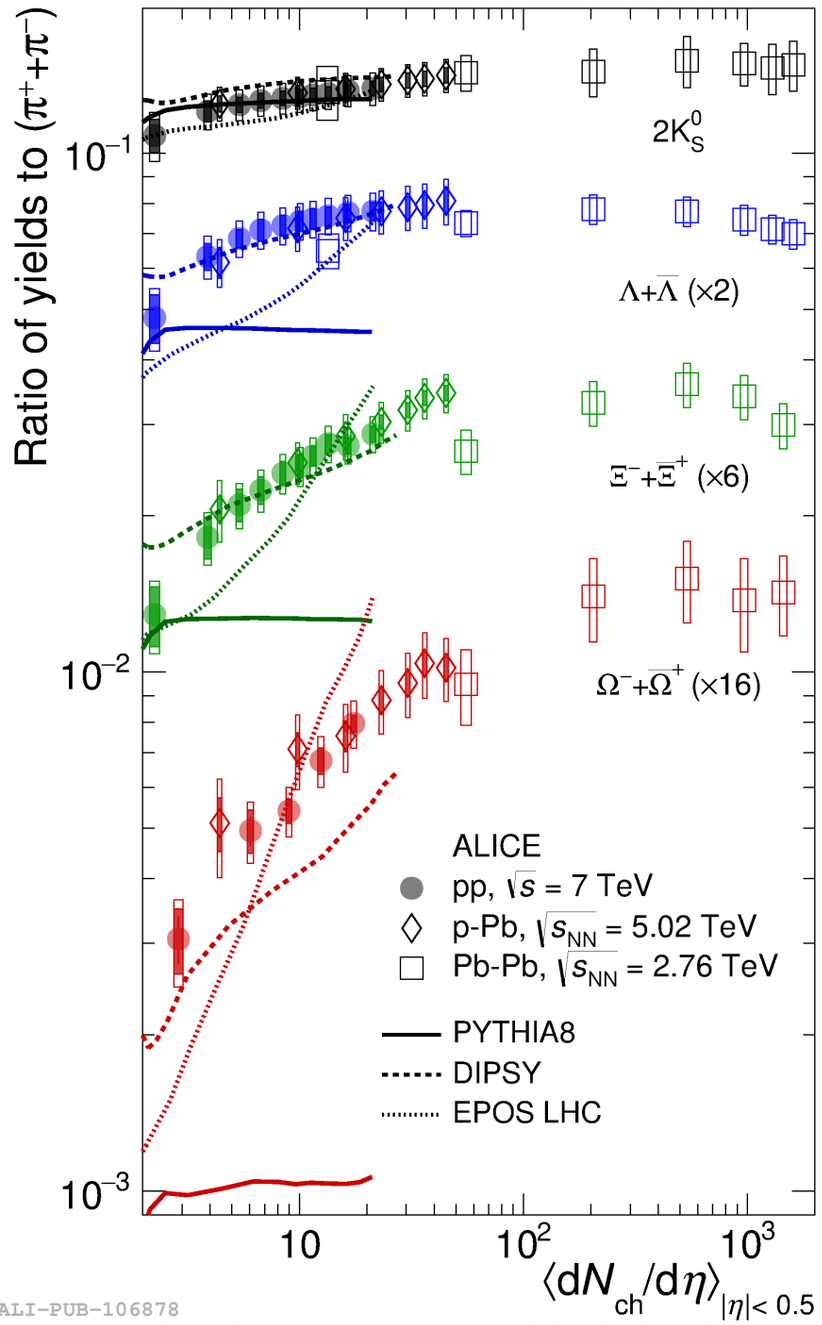

[1] Nature Physics 13 (2017) 535-539
[2] CMS, JHEP 09 (2010) 091

Collective flow

Minimum bias (MB)

High-multiplicity (HM)

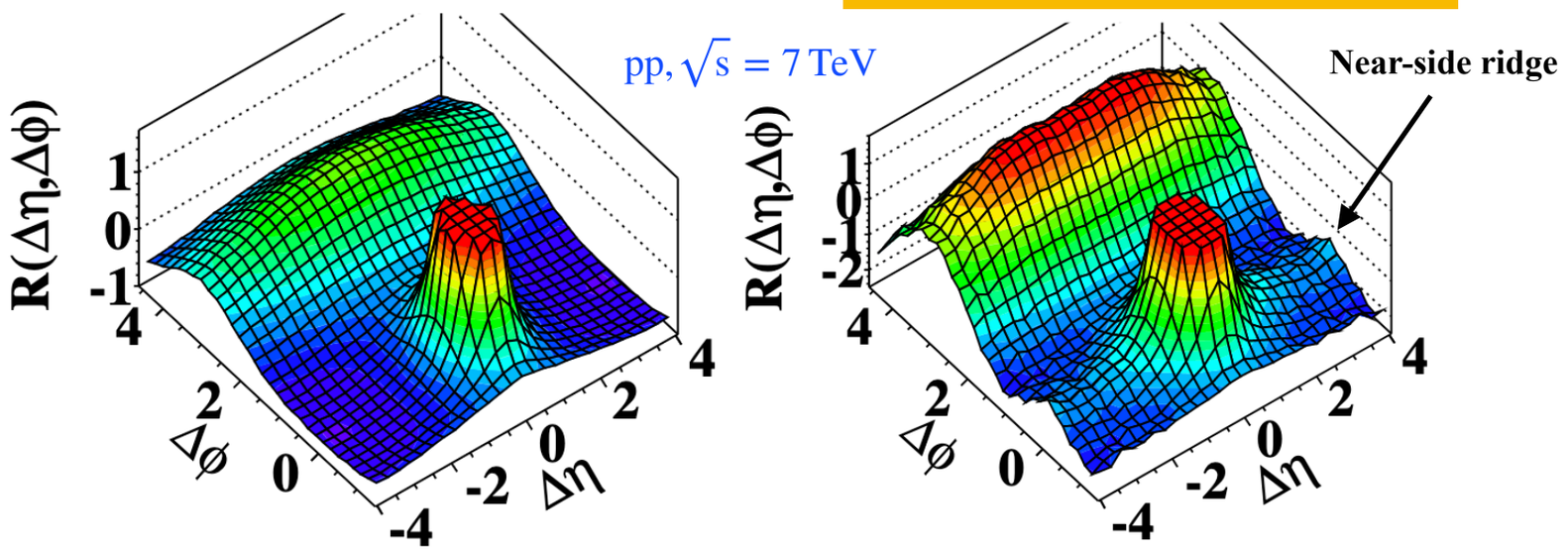

Enhancement of strange hadron production [1] and ridge structure in high multiplicity pp collisions [2]

No conclusive results on jet quenching in high-multiplicity pp collisions (based on inclusive measurements)!

Need further investigation through jet substructure observables: more sensitive to jet-medium interaction

ALICE experimental setup

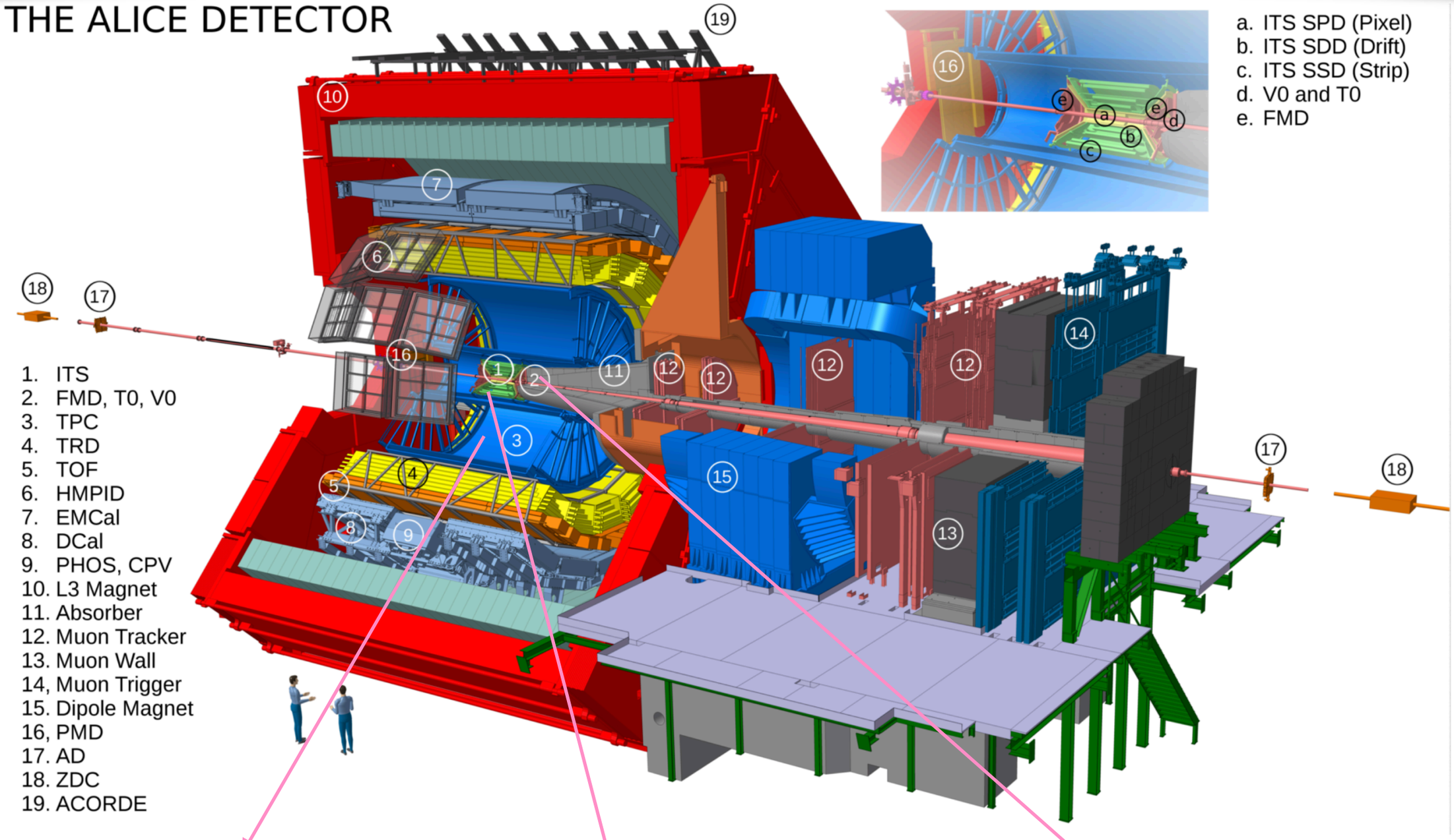

Time Projection Chamber (TPC)
Charged particle identification

Inner Tracking System (ITS)
Charged particle identification
Vertex determination

V0 scintillator detectors (V0A and V0C)
Trigger for MB and HM events

Multiplicity dependent jet results in pp collisions at $\sqrt{s}$ = 13 TeV with ALICE

Charged-jet production
Eur. Phys. J. C 82 (2022) 514

Search for jet quenching via di-jet acoplanarity
JHEP 05 (2024) 229

Charged-particle intra-jet properties
Eur. Phys. J. C (2024) 84: 1079

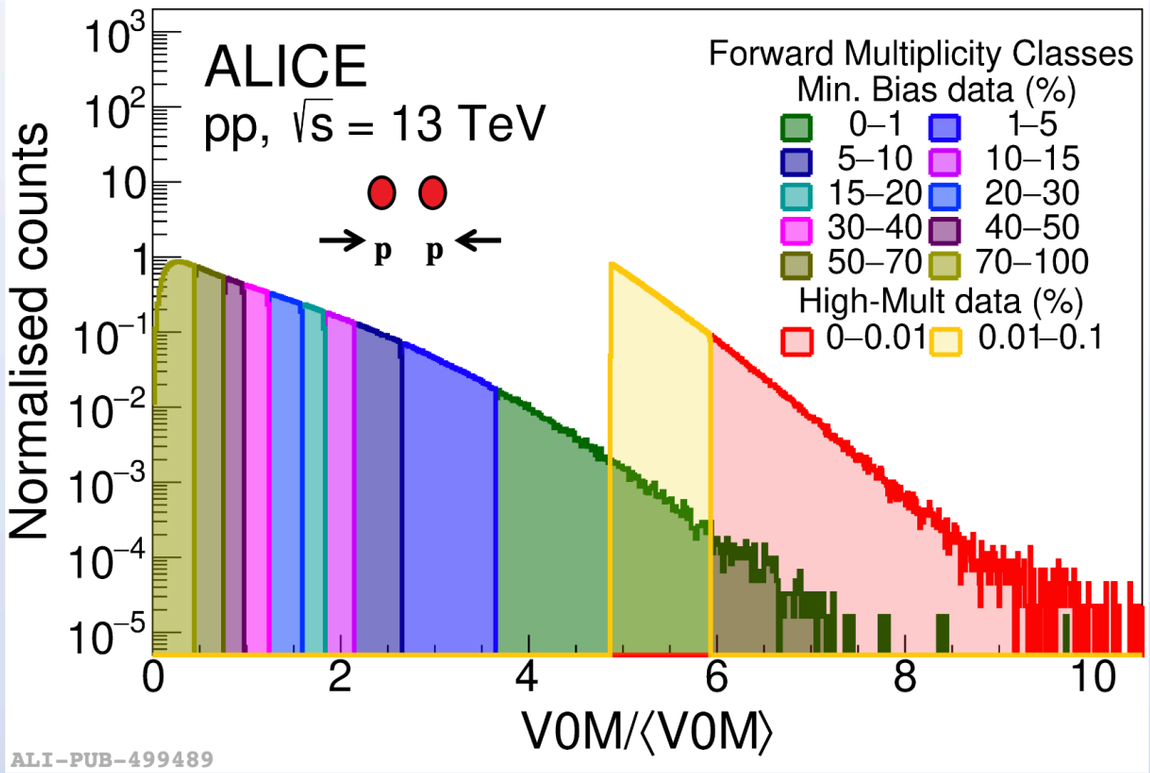

Eur. Phys. J. C 81 (2021) 630

Different multiplicity events are selected using forward detectors (V0A and V0C) to avoid auto correlations between event activities and jet measurements.

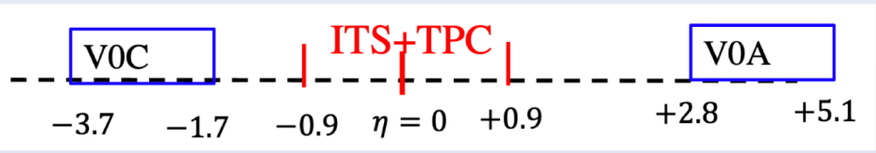

Event activity categorization: V0M = V0A + V0C

<V0M> = Mean of minimum bias V0M distributions

High Multiplicity (HM): 5 < V0M/< V0M > < 9 (used for jet shape observables)

Jet measurements: ITS + TPC

➢ Multiplicity classes are determined using V0M amplitude distribution

Multiplicity dependent jet results in pp collisions at $\sqrt{s}$ = 13 TeV with ALICE

Charged-jet production

Eur. Phys. J. C 82 (2022) 514

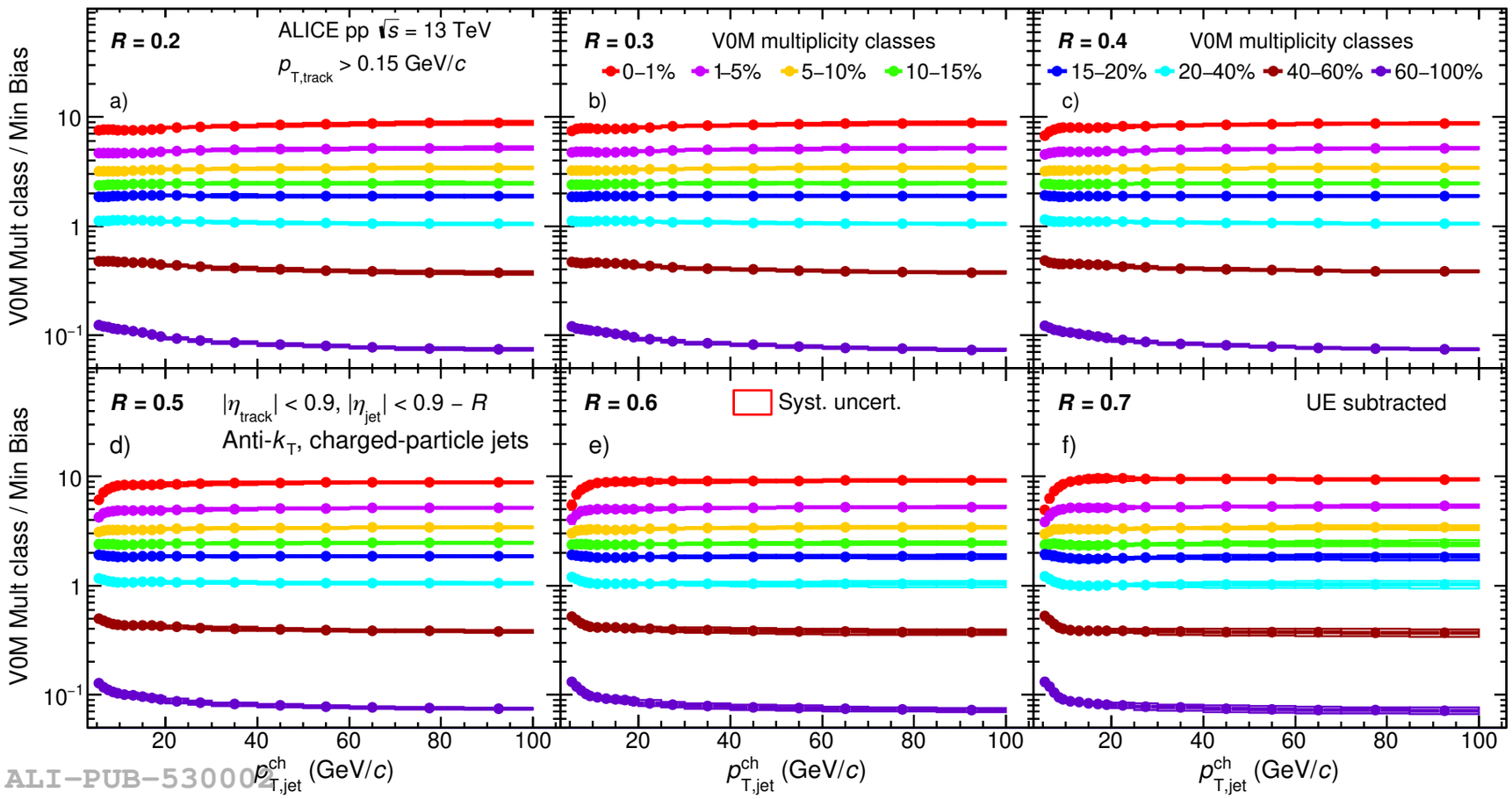

- **A higher (lower) jet yield is observed in higher (lower) multiplicity classes, but the slope of the spectrum stays similar to the one measured in MB.**
- **The charged-particle jet yield ratio is independent of the jet resolution parameter R and jet p_T.**

Multiplicity dependent jet results in pp collisions at $\sqrt{s}$ = 13 TeV with ALICE

Search for jet quenching via di-jet acoplanarity

JHEP 05 (2024) 229

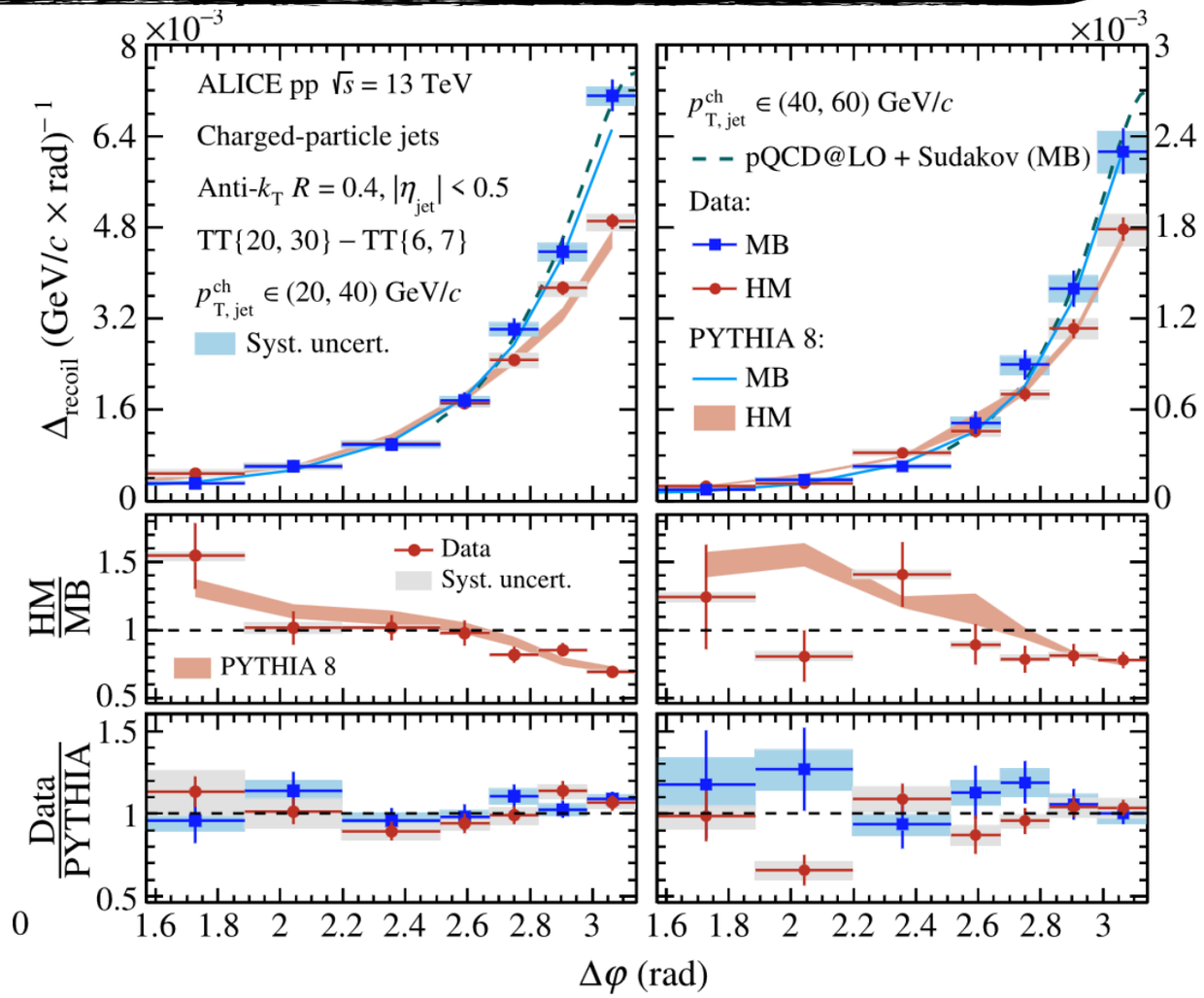

- **The jet-yield suppression in HM events occurs predominantly in the back-to-back configuration**
- **The total yield is suppressed, while the azimuthal distribution is broadened; arise from jet quenching, medium-induced jet scattering occurs in HM event**
- **HM selection bias: enhanced multiple jets**

Multiplicity dependent jet results in pp collisions at $\sqrt{s}$ = 13 TeV with ALICE

Charged-jet production
Eur. Phys. J. C 82 (2022) 514

Search for jet quenching via di-jet acoplanarity
JHEP 05 (2024) 229

Charged-particle intra-jet properties
Eur. Phys. J. C (2024) 84: 1079

Challenges:

- **The modification is really coming from QGP, or something else?**
- **Proper underlying event subtraction!**
- **Application of standard correction procedure!**

What will happen if one changes the jet radius parameter (Jet R)?

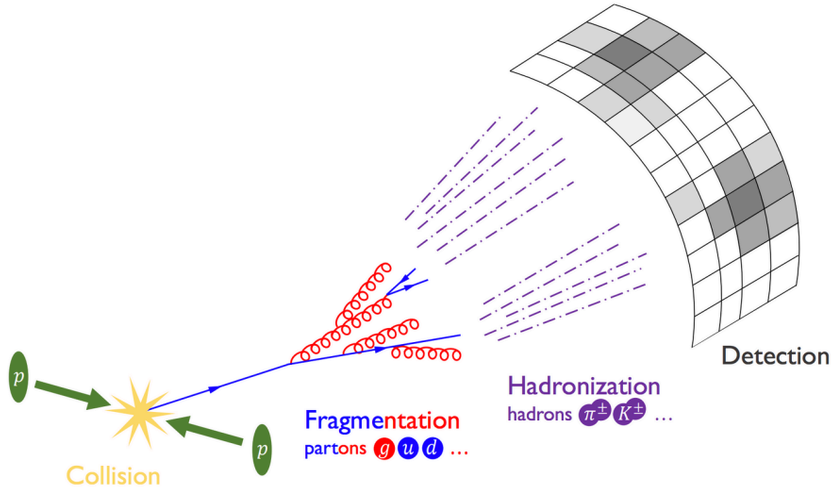

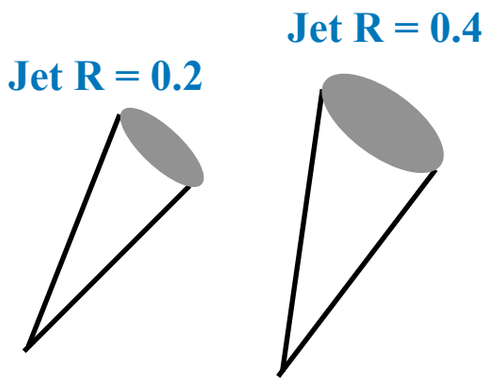

Large jet R covers more interactions!

Analysis method and jet observables

Jet observables

Mean charged-particle multiplicity within a leading jet cone

$$< N_{ch} > = \frac{1}{N_{jets}} \sum_{i=1}^{N_{jets}} N_i$$

N_{jets} = total number of jets and N_i = number of particles within the jet

Jet fragmentation functions

$$z^{ch} = \frac{p_T^{track}}{p_T^{jet}}$$

$$\xi^{ch} = ln(\frac{1}{z^{ch}})$$

p_T^{track} = transverse momentum of track
p_T^{jet} = transverse momentum of jet

Analysis details

Track selection:
Charged-tracks, transverse momentum (p_T) > 0.15 GeV/*c*,

Jet selection:
Anti-k_T jet finding algorithm, jet radius (R) = 0.2, 0.3, 0.4,
Jet p_T = 5 - 110 GeV/*c*,
Leading jet: highest-p_T jet in an event

Correction procedure:
Bayesian Unfolding: RooUnfold
Underlying event subtraction

Systematic uncertainty:
Major contributions from Tracking inefficiency and Monte Carlo (MC) dependence

✓Related to parton shower processes
✓Distribution of final state particles resulting from jet

Background Subtraction

Jet observables (Generated level) → **Detector response** → **Jet observables (Reconstructed level)**

Unfolding: 4D response matrix

Axis 1: Jet p_T^{rec} Axis 2: Observable^{rec}

Axis 3: Jet p_T^{gen} Axis 4: Observable^{gen}

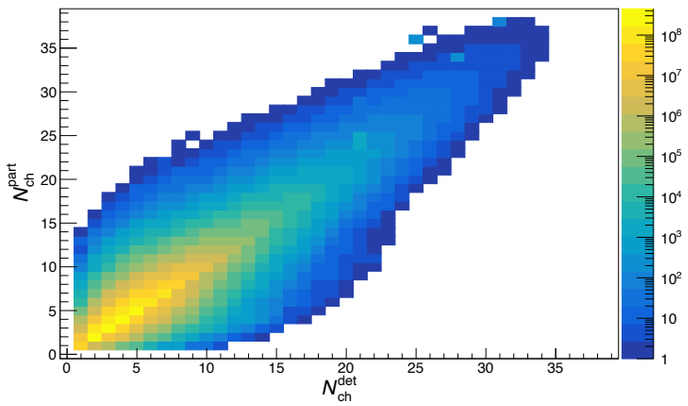

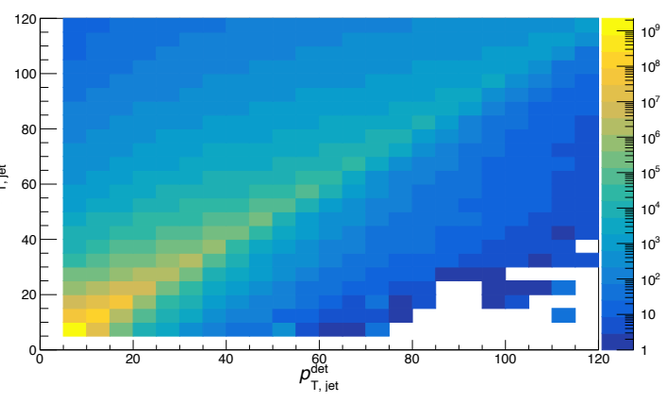

Performance of unfolding method

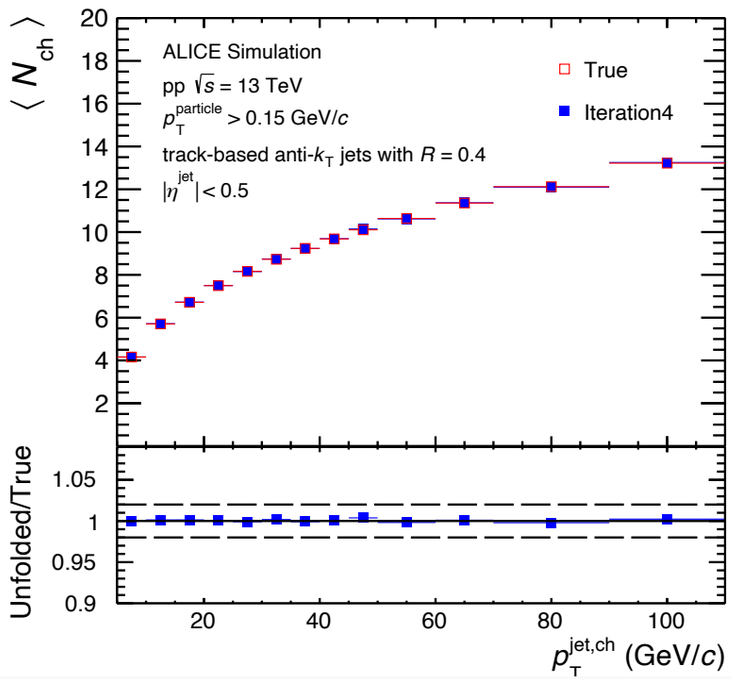

Unfolded results show good agreement with gen (truth)-level results

Underlying events (UE) in pp collisions

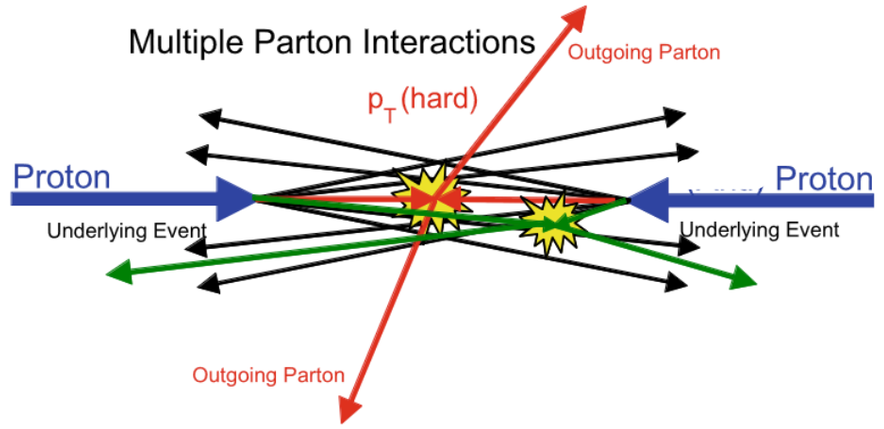

UE estimation: perpendicular cone method

UE subtraction: on a statistical basis after unfolding

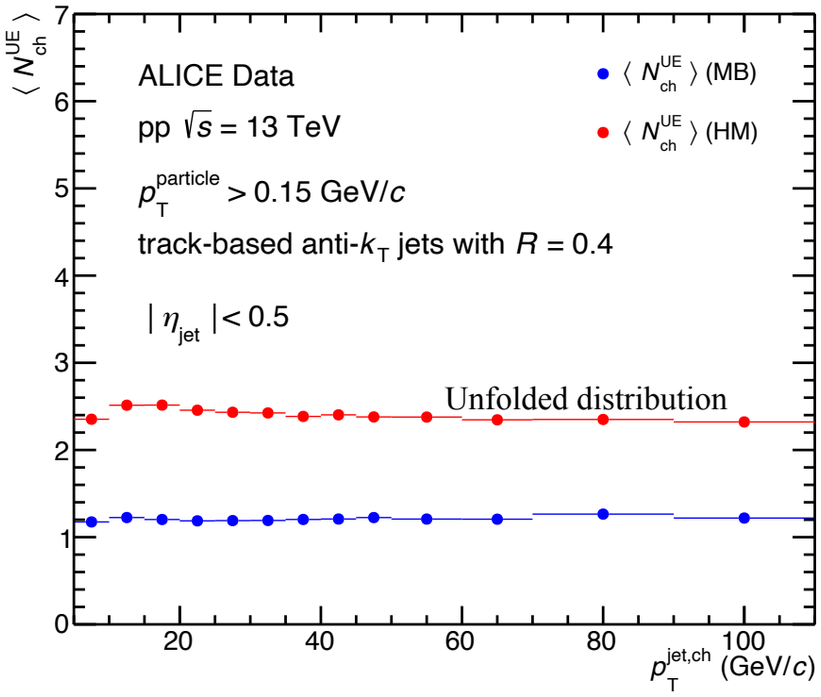

Results and Discussions

$< N_{ch} >$

Minimum bias (MB)

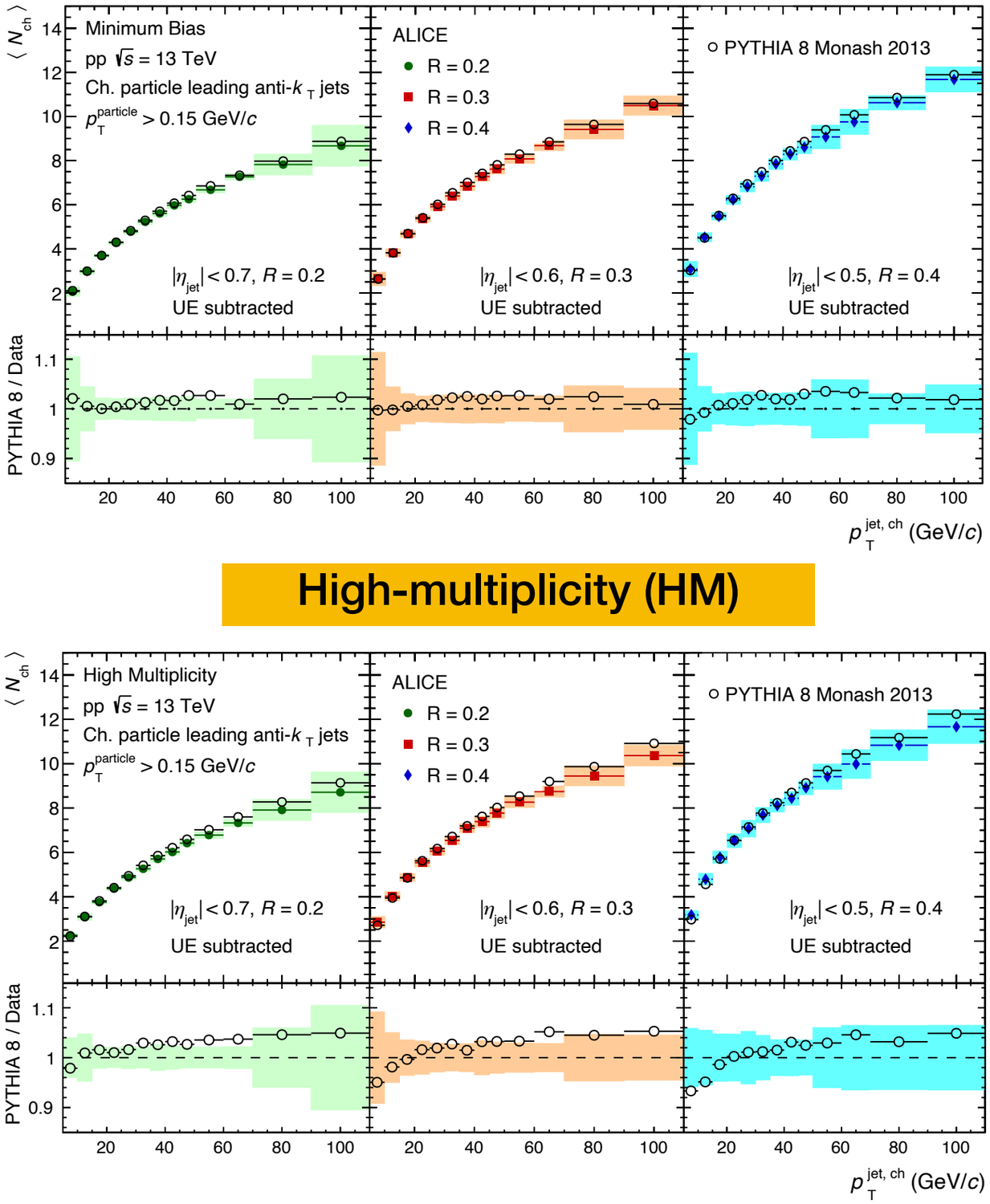

HM/MB

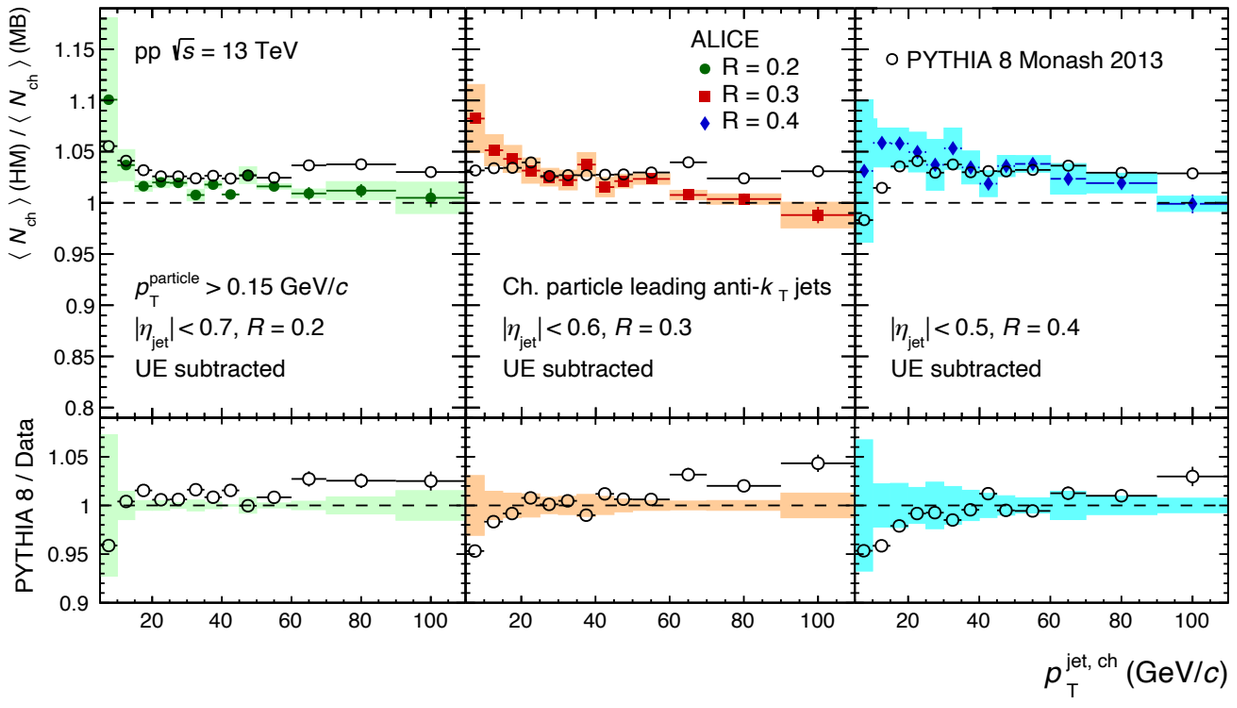

High-multiplicity (HM)

- $<N_{ch}>$ rises monotonically with increasing p_T^{jet}
- $<N_{ch}>$ increases with increasing jet radius R
- $<N_{ch}>$ is slightly large in HM compared to that in MB (e.g. ~ 5% [$p_T^{jet} < 60$ GeV/c, $R = 0.4$]) (Hint of jet modification!)
- Pythia 8 reproduces the distributions for both HM and MB within systematic uncertainties
- Pythia 8 slightly deviates from the data in HM/MB beyond systematic uncertainty

Results and Discussions

z^{ch}

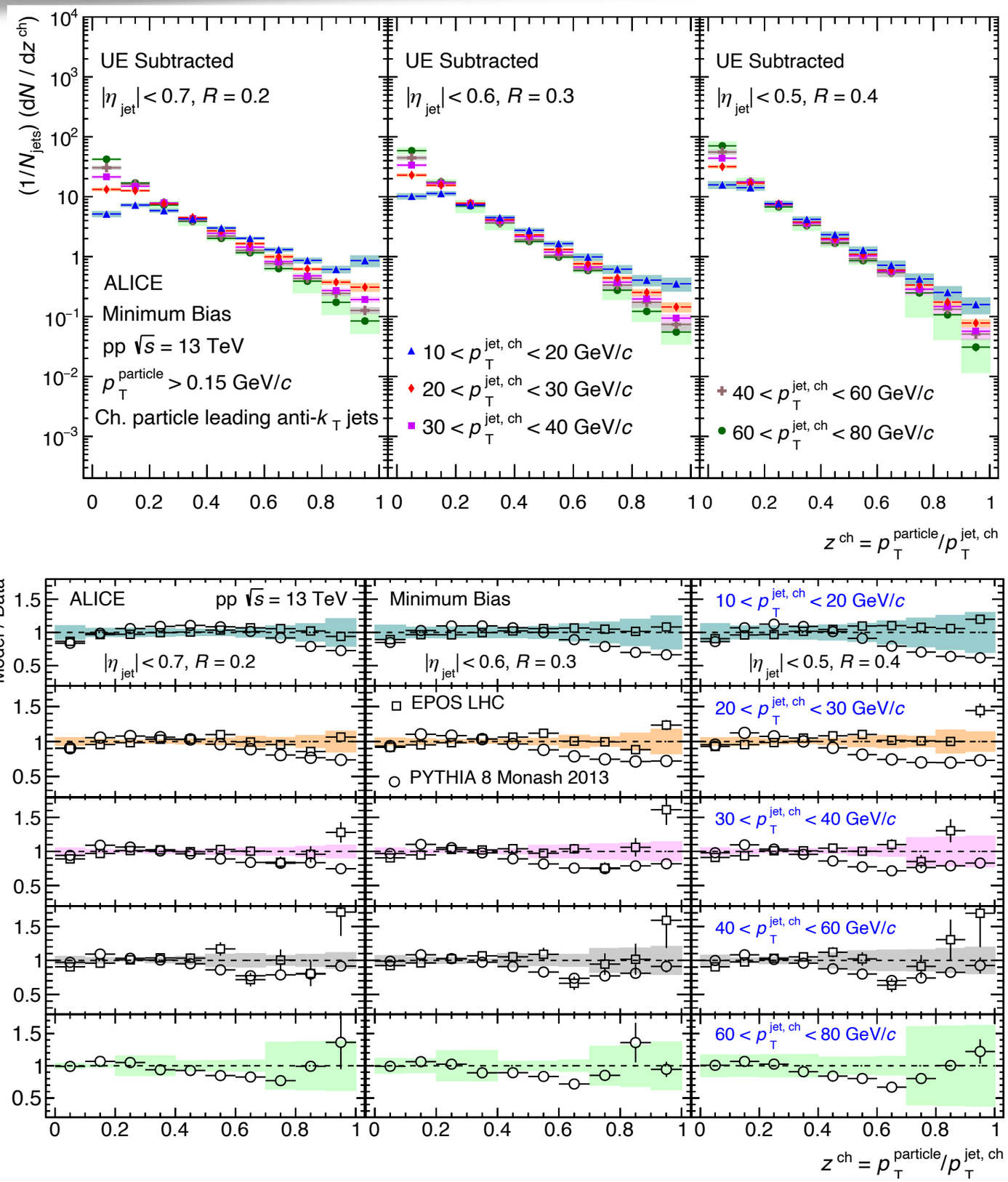

Jet fragmentation: jet p_T dependence

✓Scaling with jet p_T: Indication of jet p_T independent jet fragmentation for wider jets

MC predictions:

✓PYTHIA 8 describes the data within systematic uncertainty for lower and higher jet p_T ranges

✓PYTHIA 8 underestimate the data for intermediate z^{ch} values for intermediate jet p_T ranges

✓EPOS LHC reproduces the data better compared to PYTHIA 8 within systematic uncertainty

Similar observations for HM events

Results and Discussions

z^{ch}

HM/MB (10-20 GeV/c)

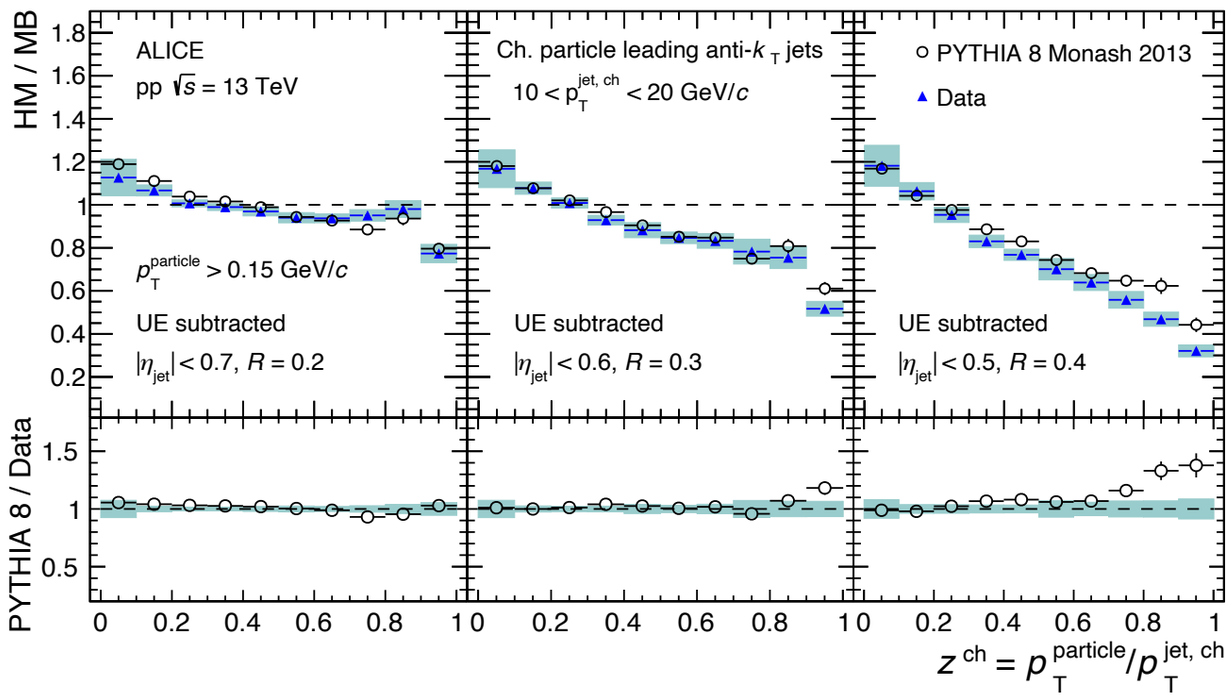

HM/MB (30-40 GeV/c)

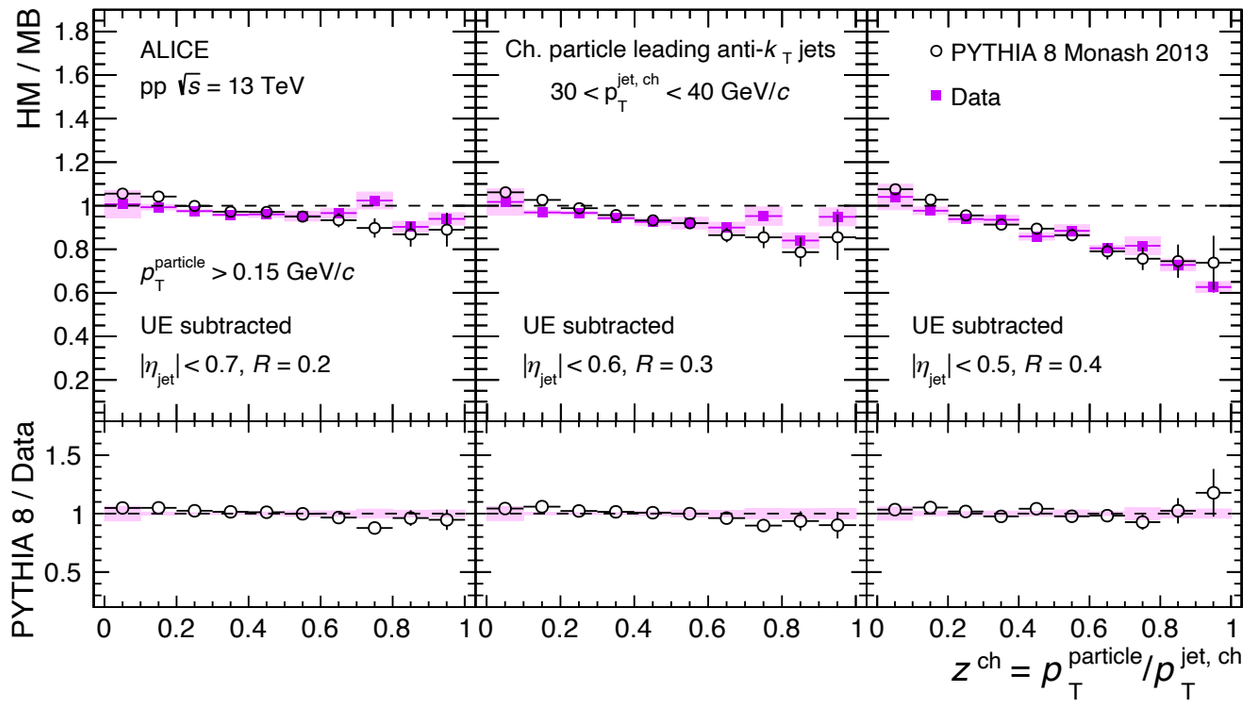

HM/MB (60-80 GeV/c)

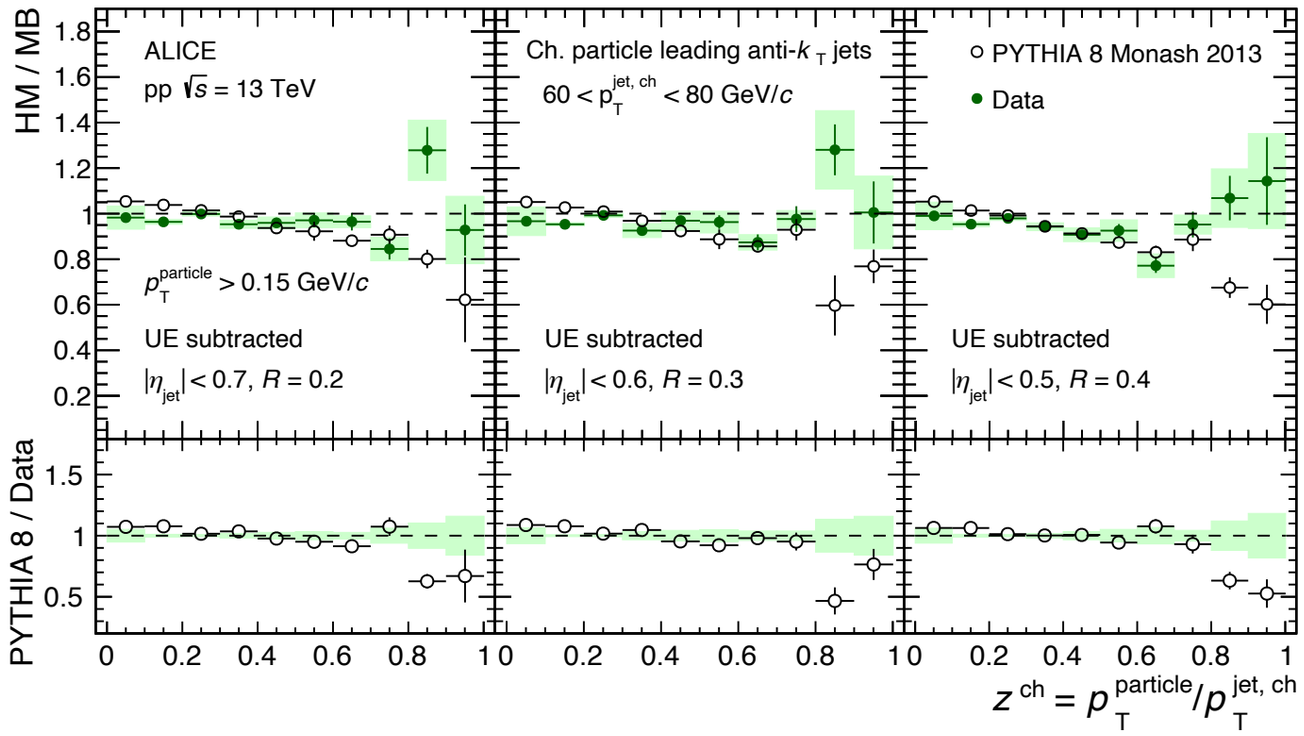

Modification in jet fragmentation!

PYTHIA 8 describes the data within systematic uncertainty except for high jet p_T (60-80 GeV/c), jet $R = 0.4$ ($z^{ch} > 0.7$)

- Significant modification at low jet p_T (10-20 GeV/c)
- Dependence with jet p_T and jet R
- Modification reduces at high jet p_T (60-80 GeV/c)

Results and Discussions

z^{ch}

HM/MB (10-20 GeV/c)

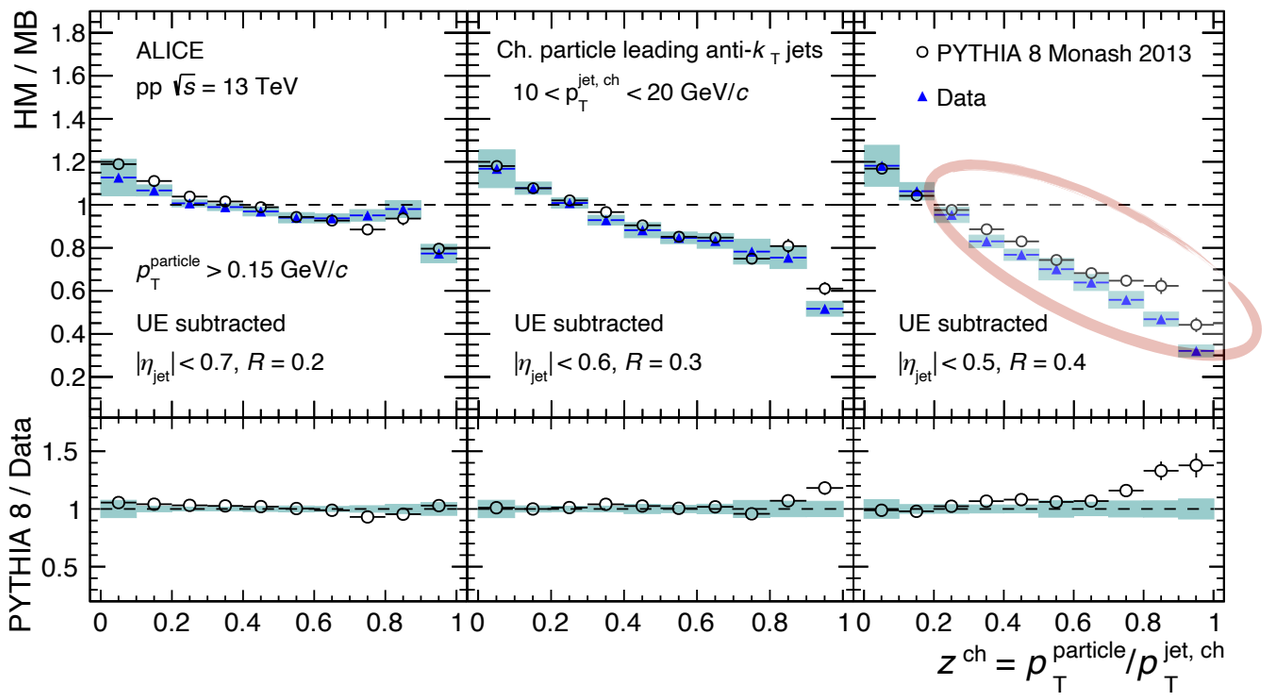

HM/MB (30-40 GeV/c)

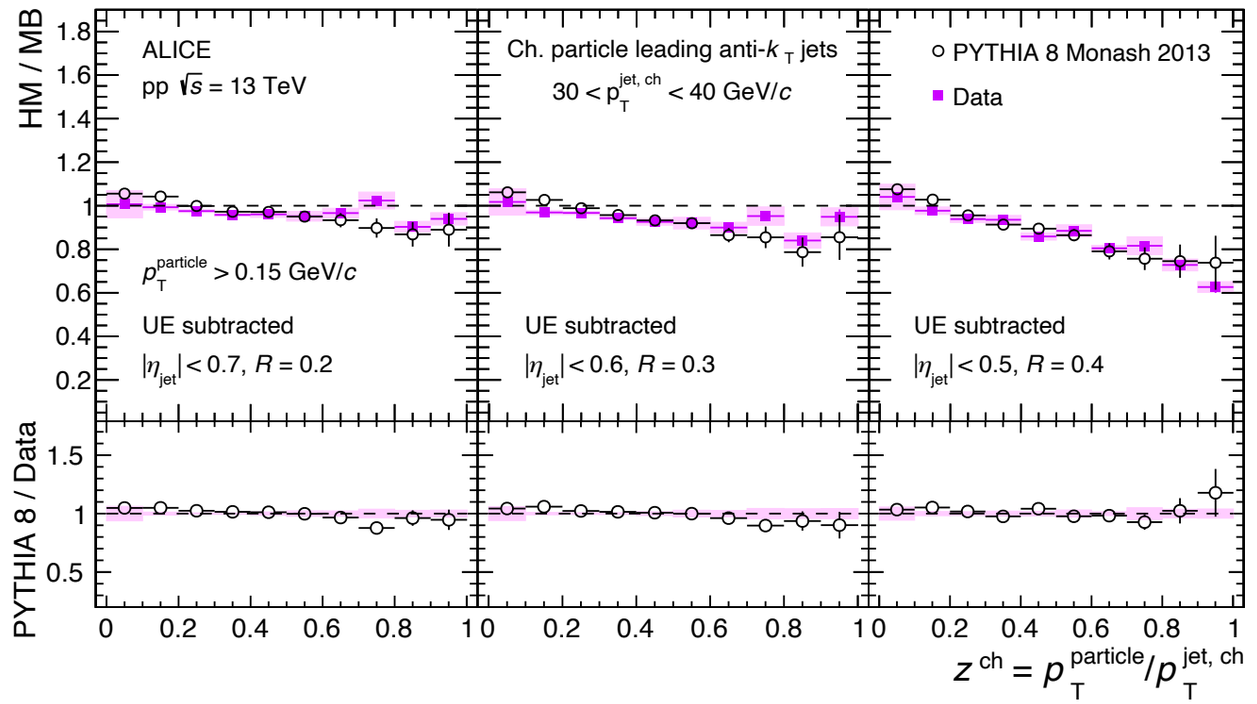

HM/MB (60-80 GeV/c)

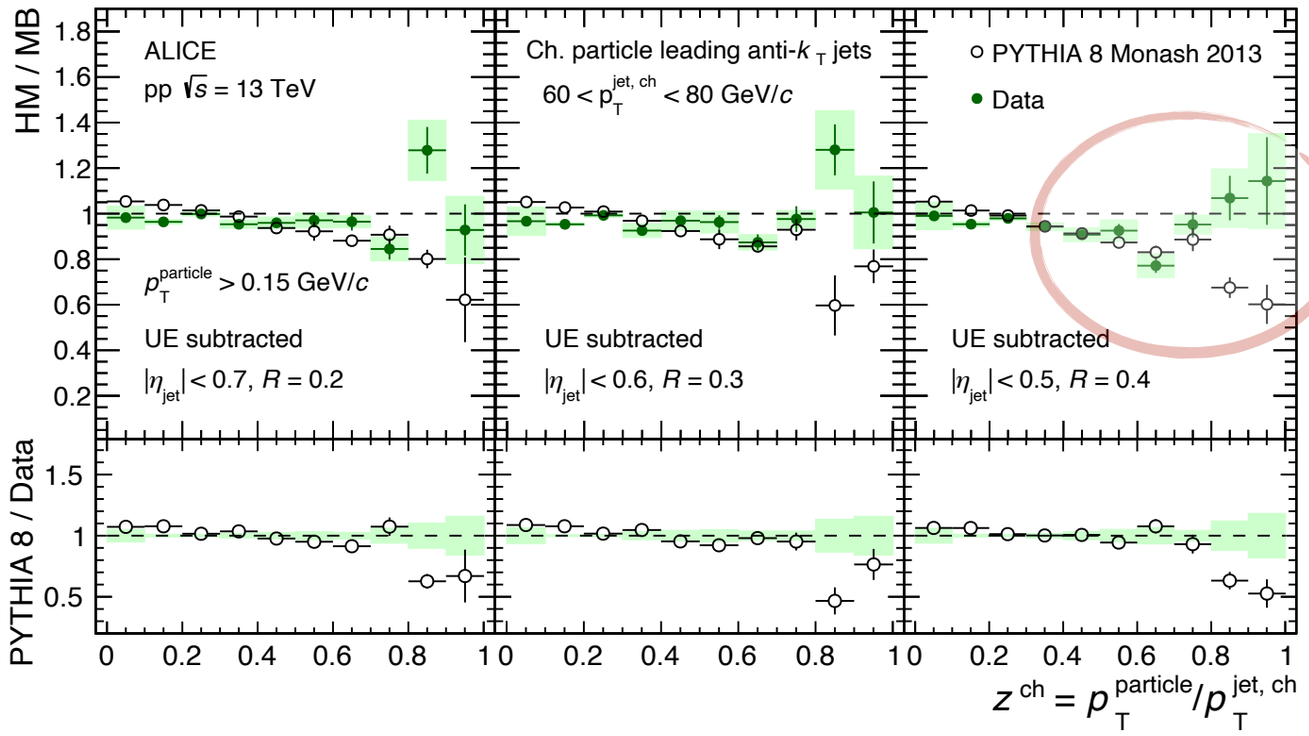

Modification in jet fragmentation!

PYTHIA 8 describes the data within systematic uncertainty except for high jet p_T (60-80 GeV/c), jet $R = 0.4$ ($z^{ch} > 0.7$)

- Significant modification at low jet p_T (10-20 GeV/c)
- Dependence with jet p_T and jet R
- Modification reduces at high jet p_T (60-80 GeV/c)

Modification of jet fragmentation: HI vs HM z^{ch}

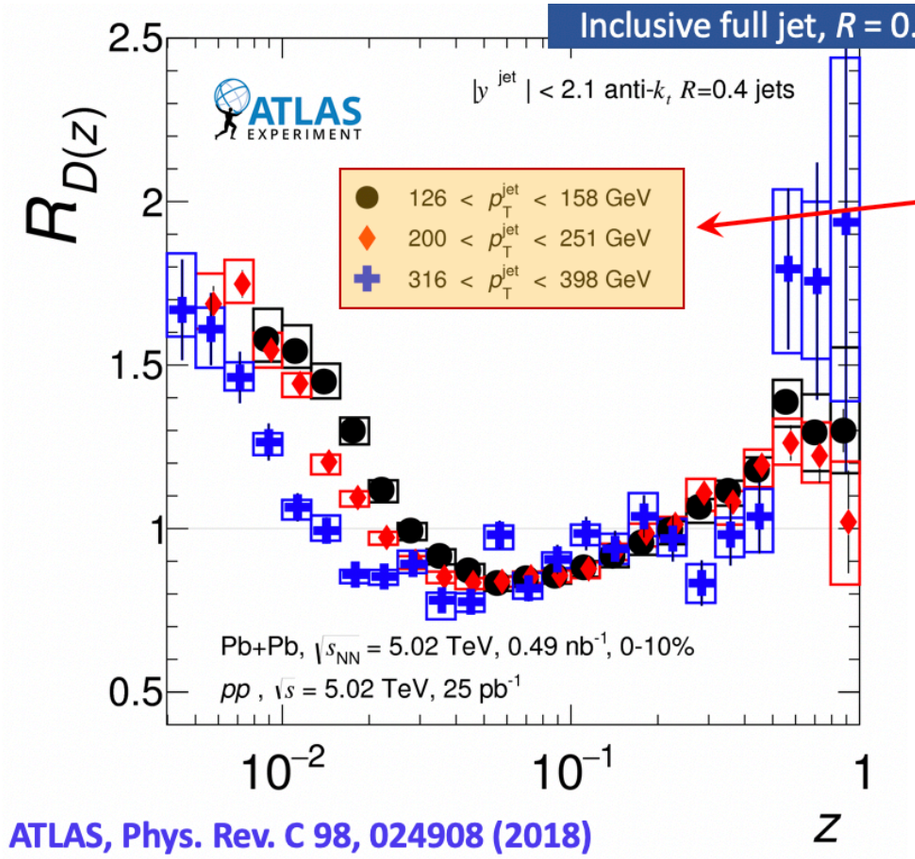

ATLAS, Phys. Rev. C 98, 024908 (2018)

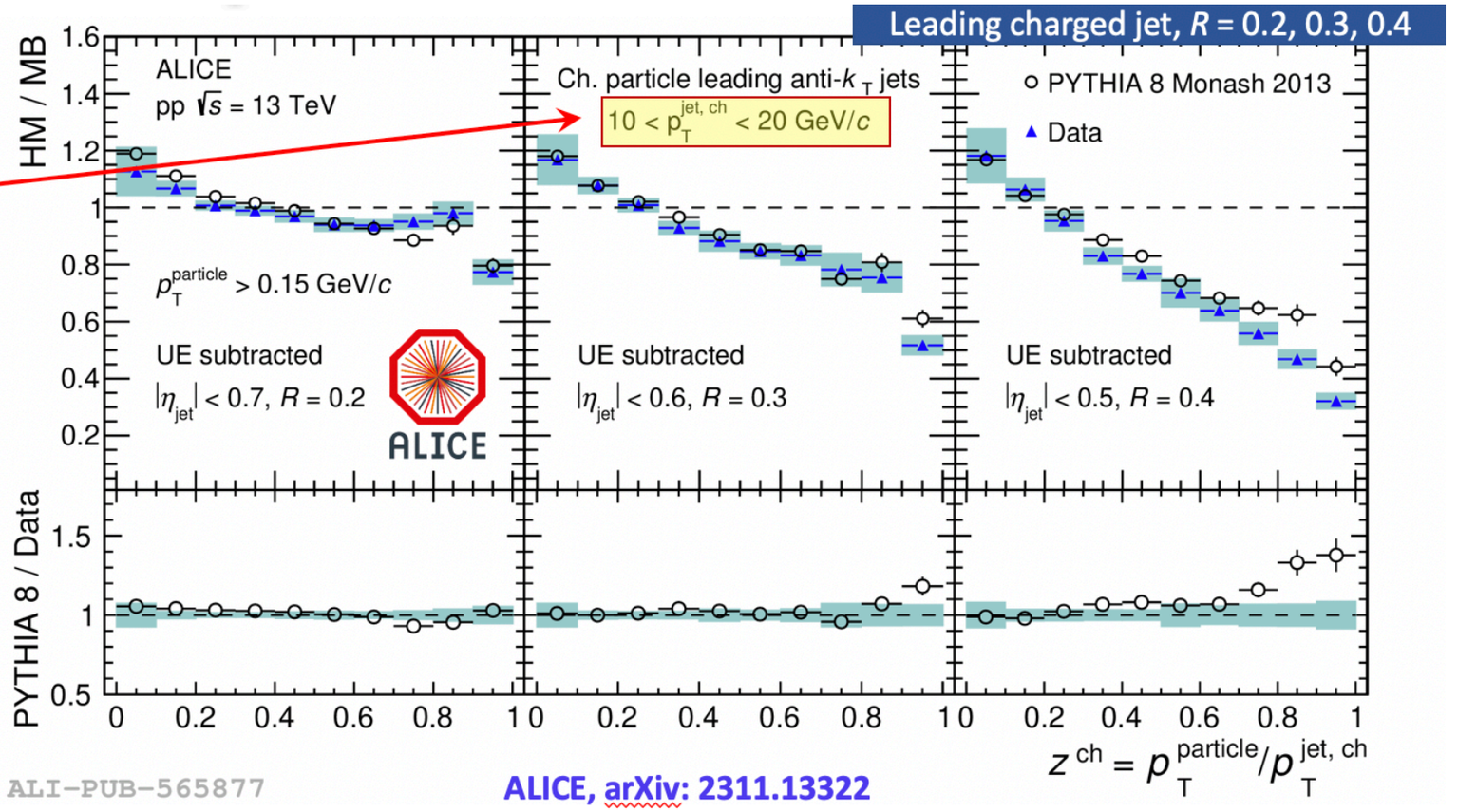

ALI-PUB-565877

ALICE, arXiv: 2311.13322

System	Jet p_T	Low z	Intermediate z	High z
Central Pb-Pb	> **126** GeV/c	Enhancement	Supression	Enhancement
HM pp	**10-20** GeV/c	Enhancement	Supression	Suppression

Modification of jet fragmentation: HI vs HM z^{ch}

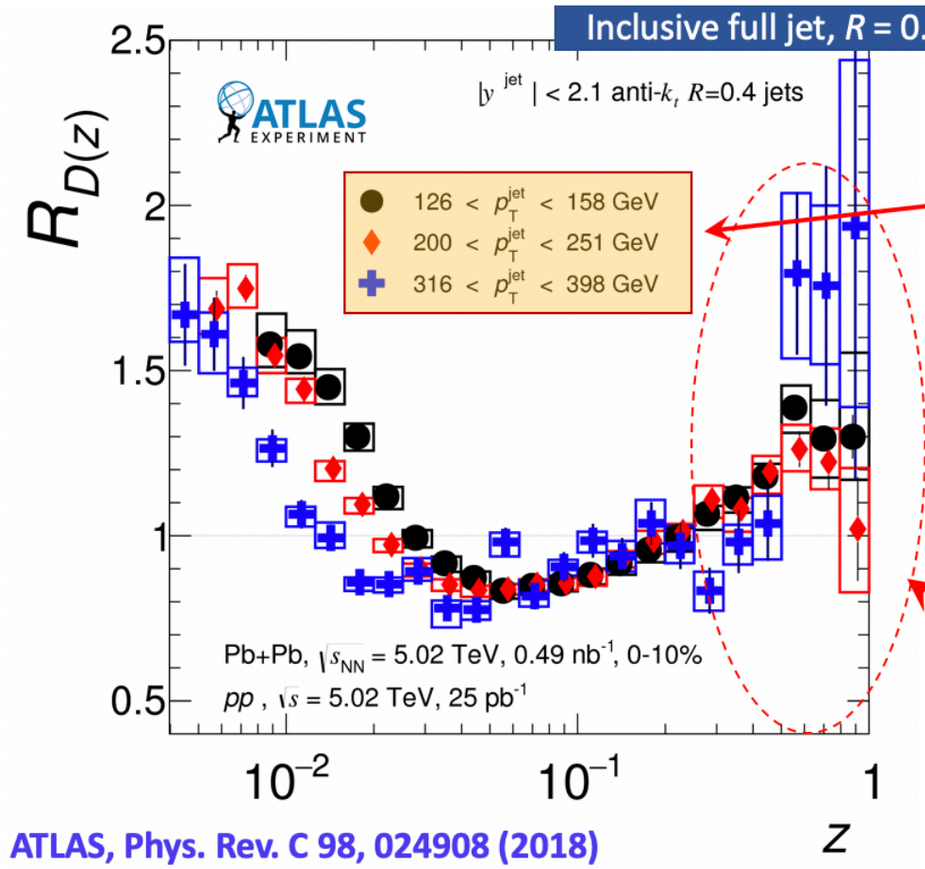

ATLAS, Phys. Rev. C 98, 024908 (2018)

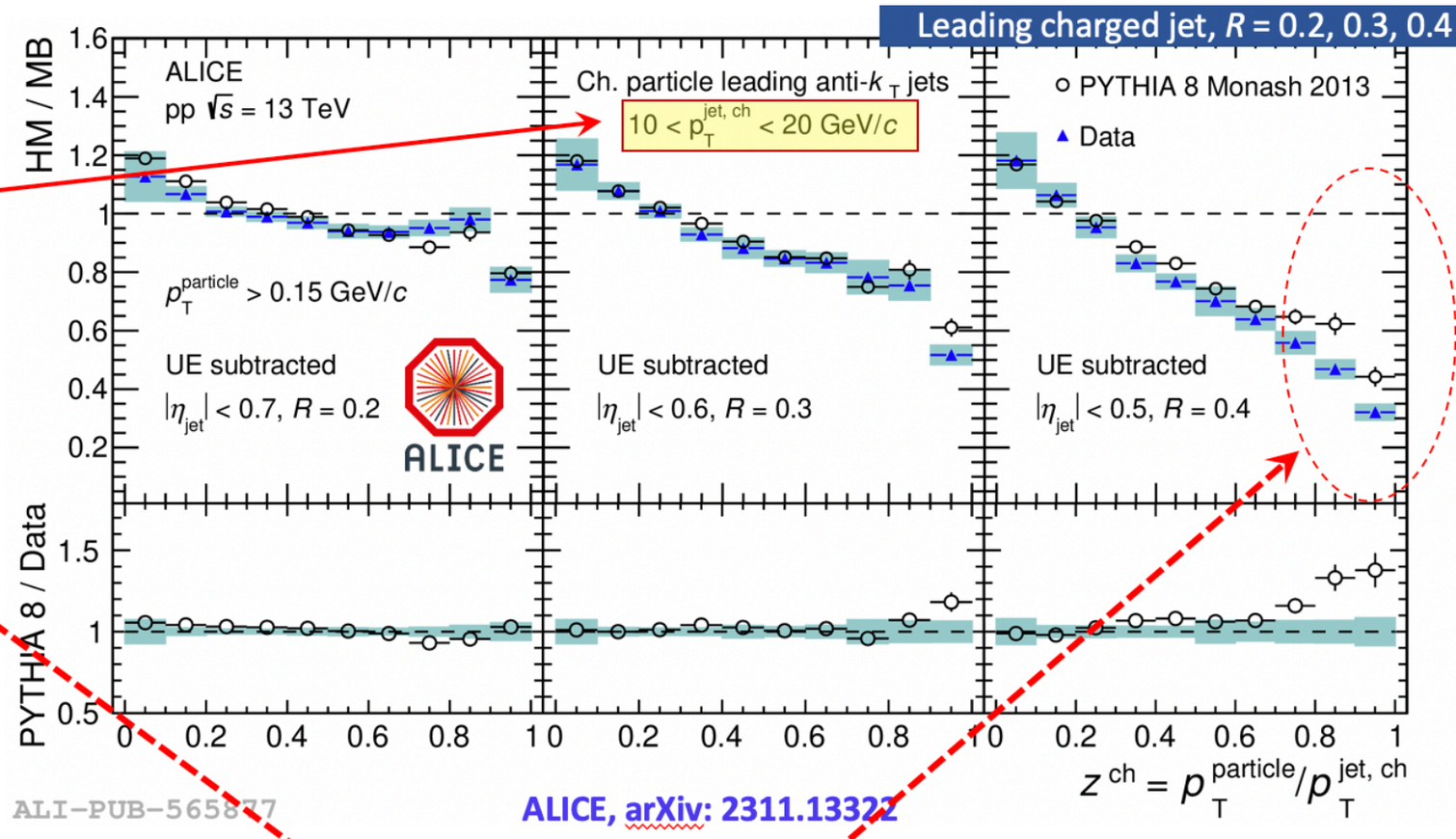

ALICE, arXiv: 2311.13322

System	Jet p_T	Low z	Intermediate z	High z
Central Pb-Pb	> **126** GeV/c	Enhancement	Supression	Enhancement
HM pp	**10-20** GeV/c	Enhancement	Supression	Suppression

Modification of jet fragmentation: HI vs HM z^{ch}

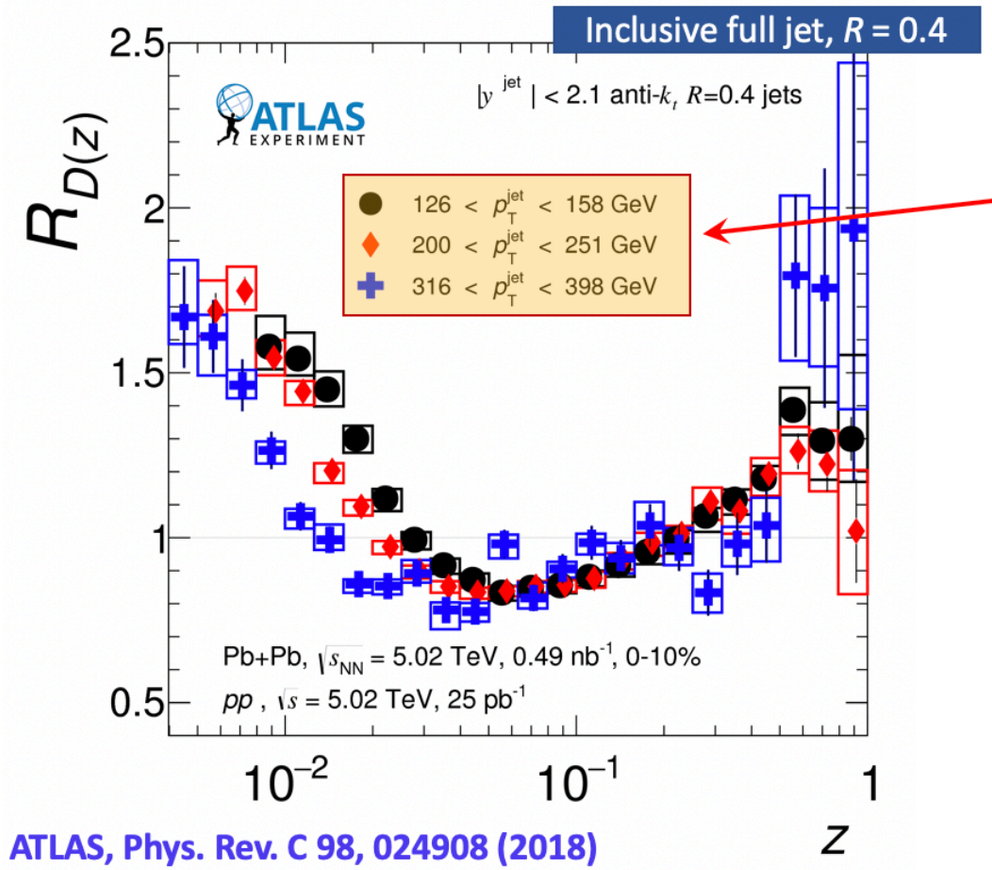

ATLAS, Phys. Rev. C 98, 024908 (2018)

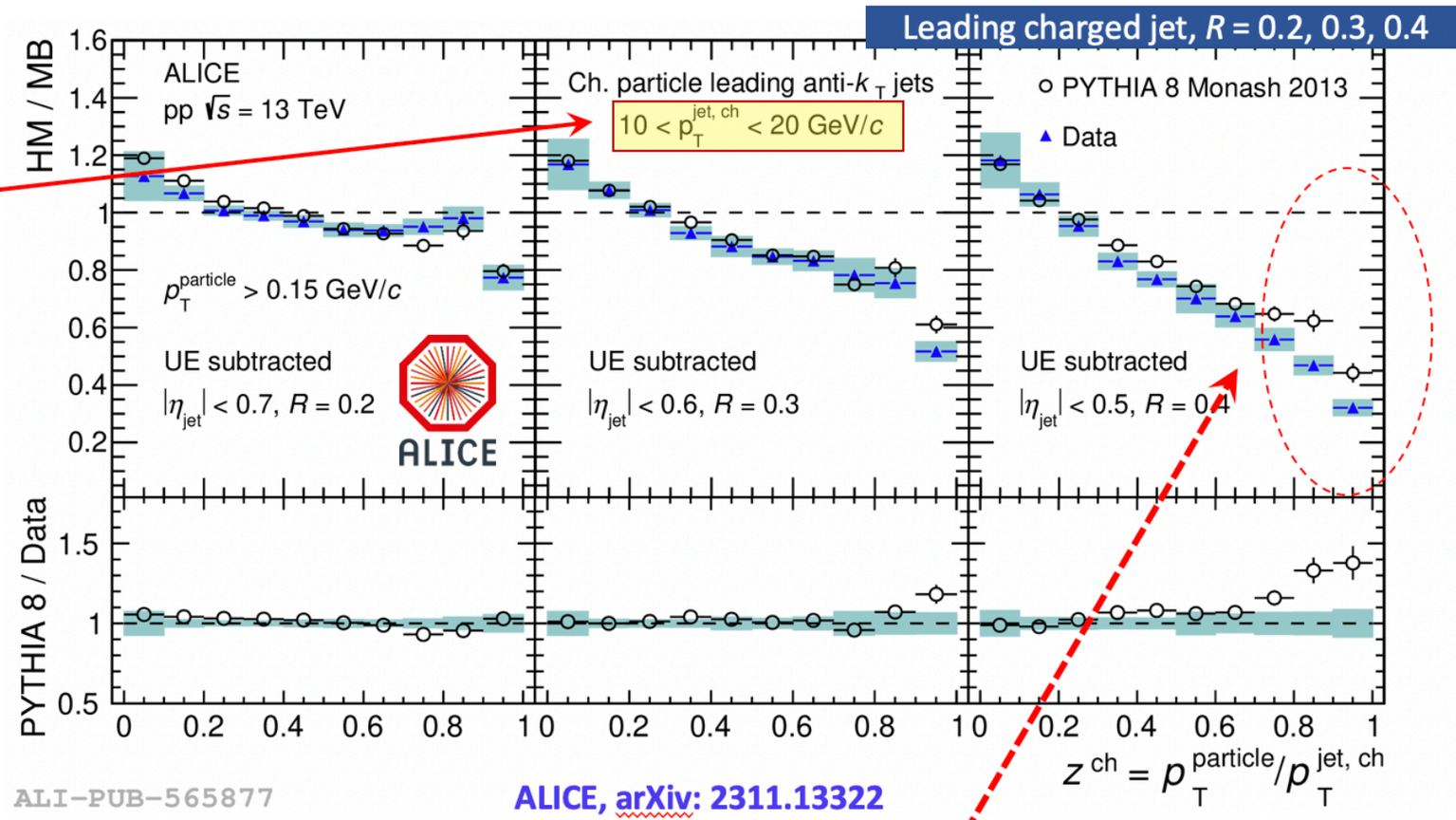

ALI-PUB-565877

ALICE, arXiv: 2311.13322

System	Jet p_T	Low z	Intermediate z	High z
Central Pb-Pb	> **126** GeV/c	Enhancement	Supression	Enhancement
HM pp	**10-20** GeV/c	Enhancement	Supression	Suppression

PYTHIA 8 shows similar trend as data in HM pp collisions → **questions the possibility of jet quenching**

Modification of jet fragmentation: HI vs HM z^{ch}

Inclusive full jet, $R = 0.4$

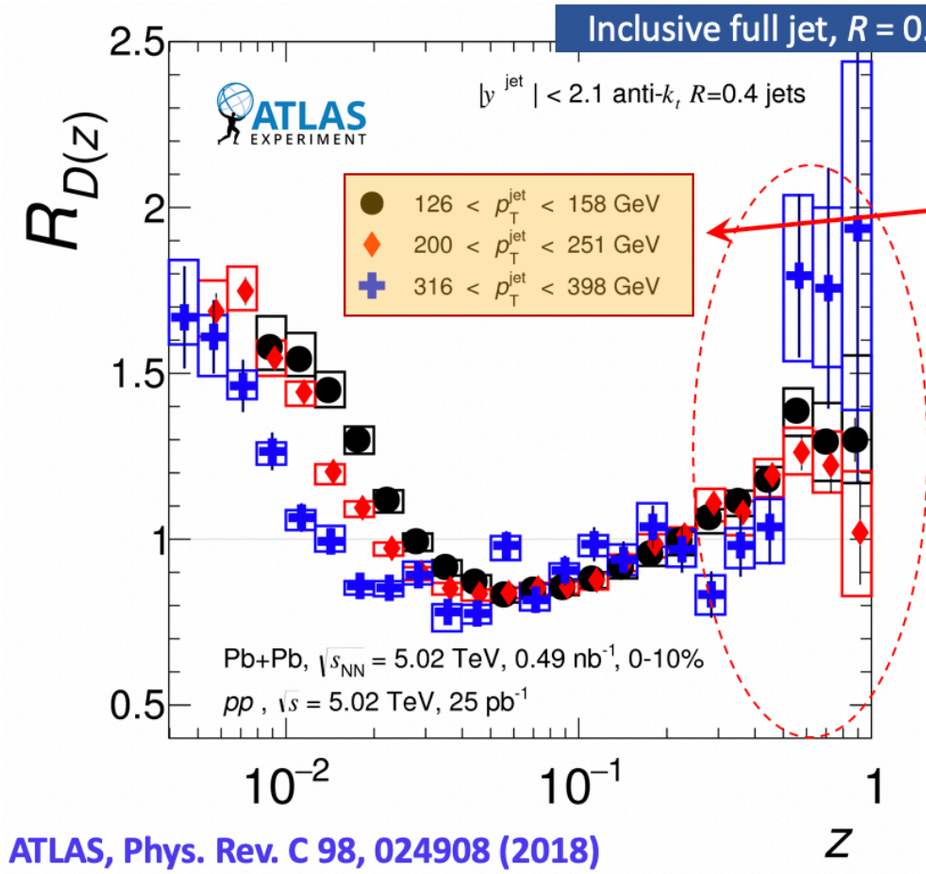

ATLAS, Phys. Rev. C 98, 024908 (2018)

Leading charged jet, $R = 0.2, 0.3, 0.4$

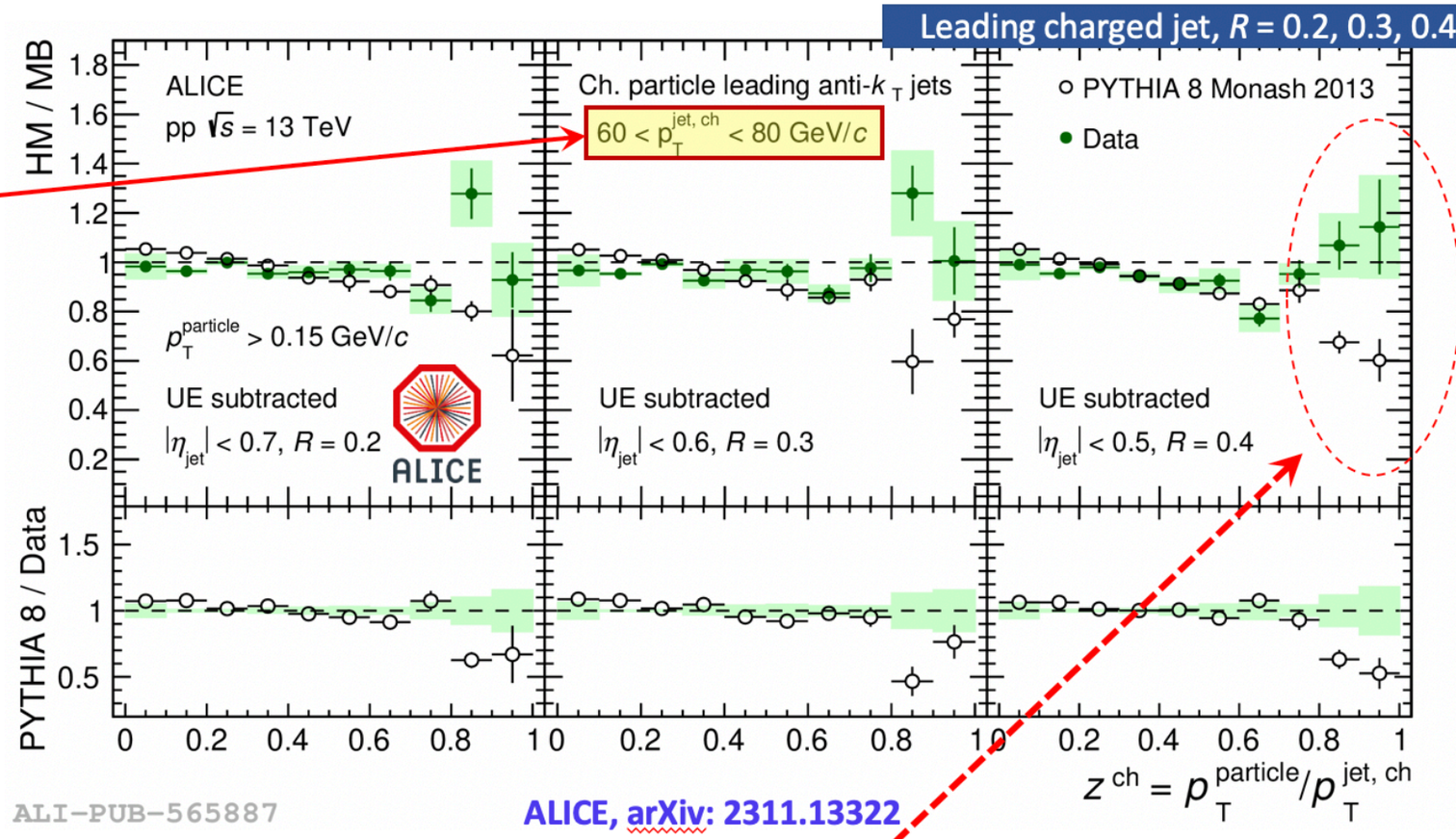

ALI-PUB-565887

ALICE, arXiv: 2311.13322

System	Jet p_T	Low z	Intermediate z	High z
Central Pb-Pb	> **126** GeV/c	Enhancement	Supression	Enhancement
HM pp	**60-80** GeV/c	No modification	Mild supression	No modification (hint of enhancement)

Modification of jet fragmentation: HI vs HM z^{ch}

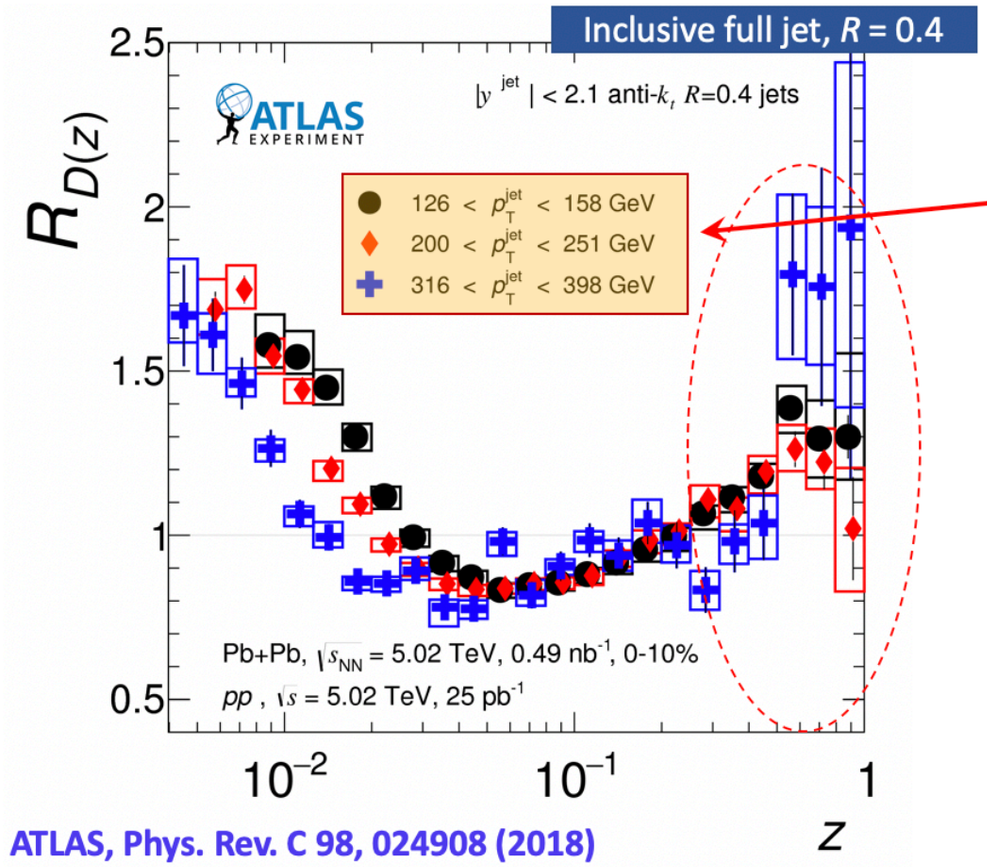

ATLAS, Phys. Rev. C 98, 024908 (2018)

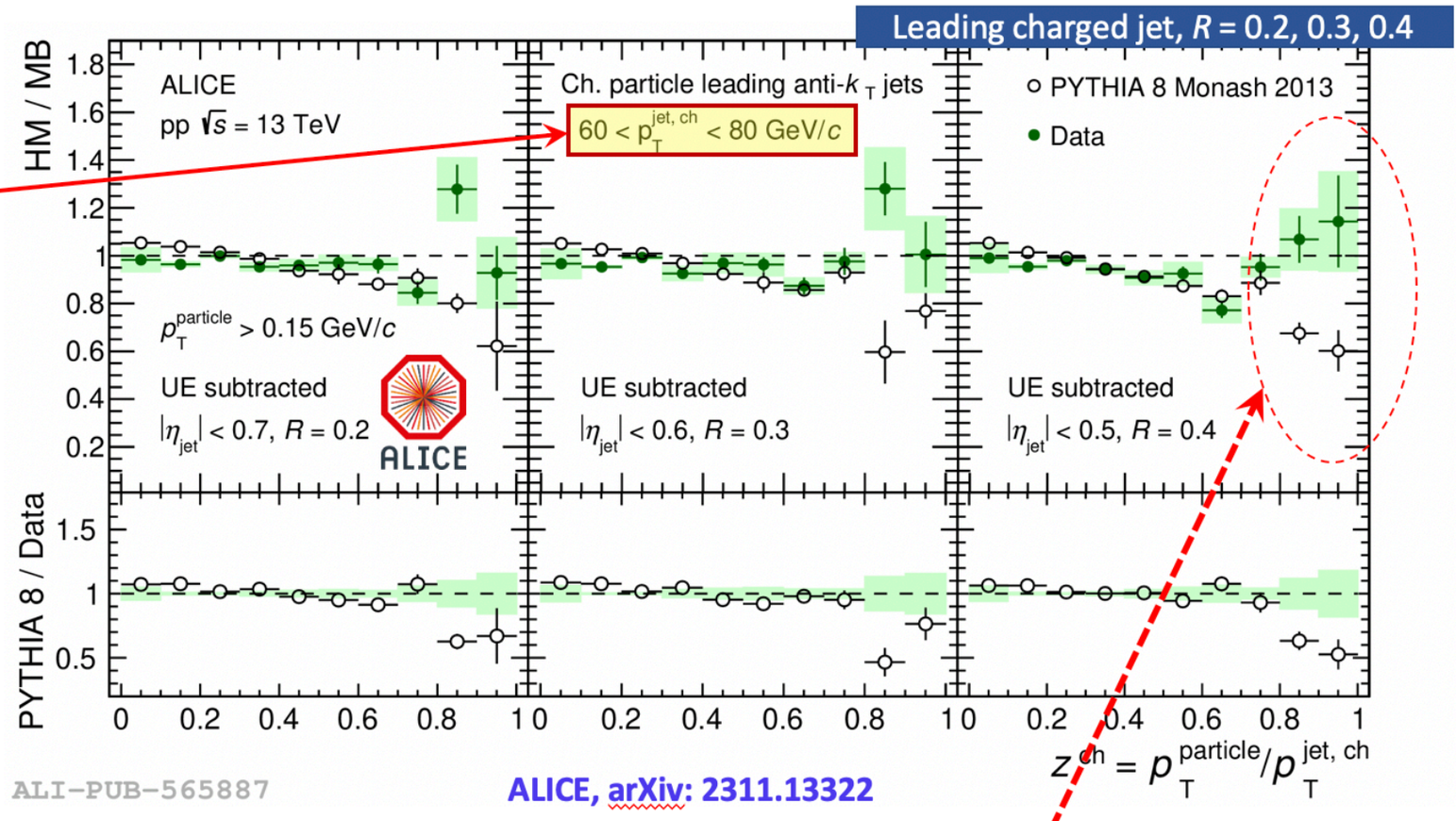

ALI-PUB-565887

ALICE, arXiv: 2311.13322

System	Jet p_T	Low z	Intermediate z	High z
Central Pb-Pb	> **126** GeV/c	Enhancement	Supression	Enhancement
HM pp	**60-80** GeV/c	No modification	Mild supression	No modification (hint of enhancement)

Data disagree with PYTHIA 8 predictions (suppression) for high p_T-jets

Modification of jet fragmentation: HI vs HM z^{ch}

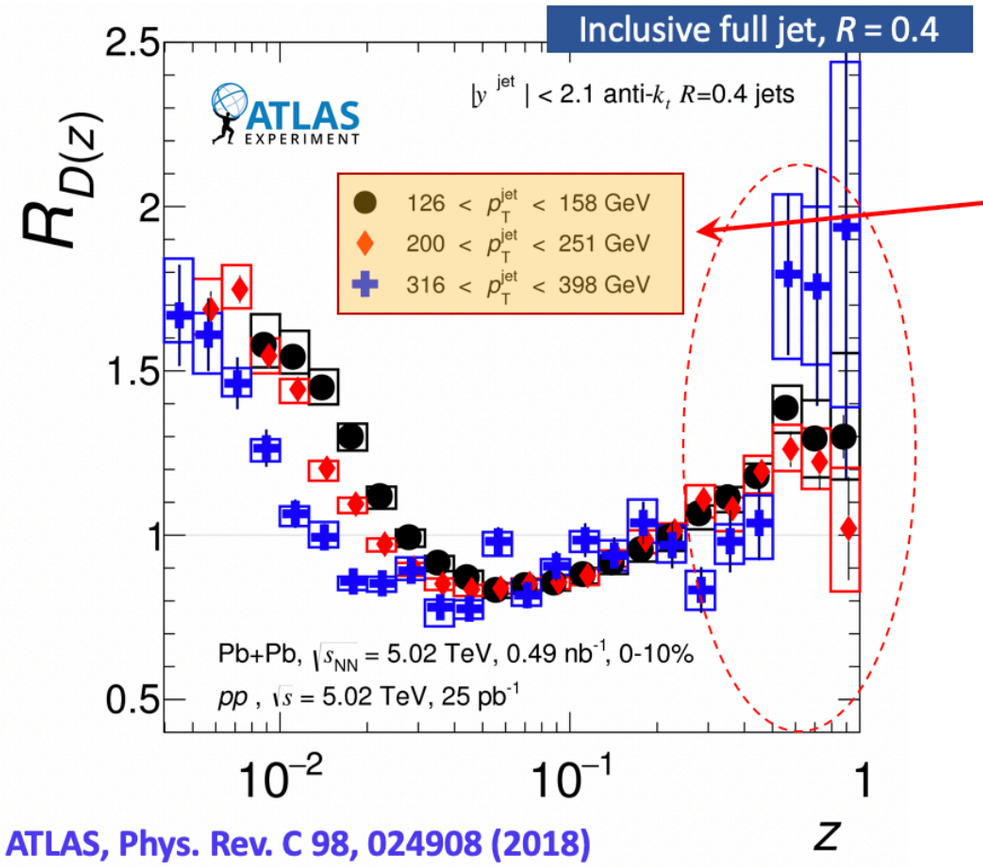

ATLAS, Phys. Rev. C 98, 024908 (2018)

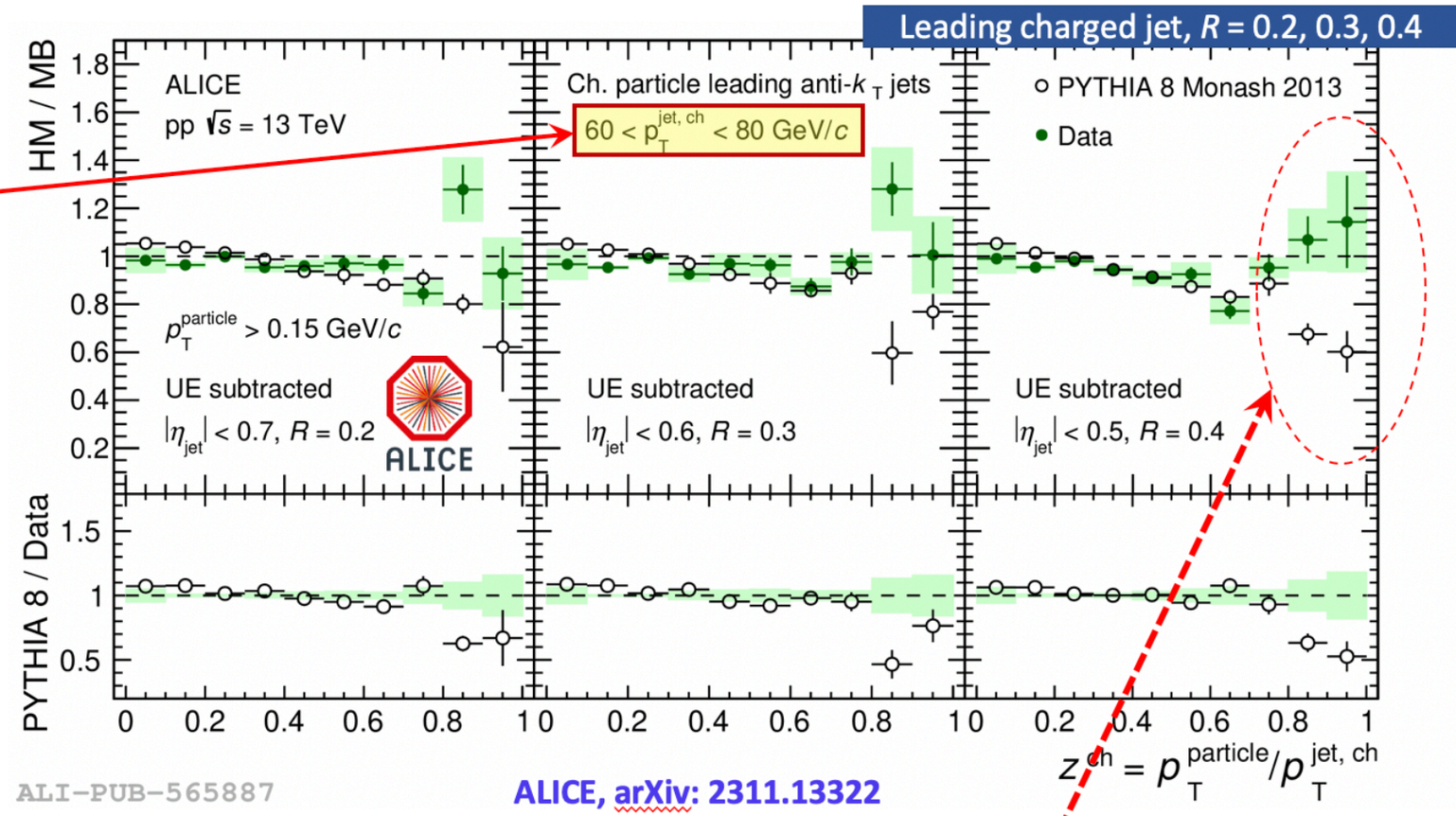

ALI-PUB-565887

ALICE, arXiv: 2311.13322

System	Jet p_T	Low z	Intermediate z	High z
Central Pb-Pb	> **126** GeV/c	Enhancement	Supression	Enhancement
HM pp	**60-80** GeV/c	No modification	Mild supression	No modification (hint of enhancement)

Data disagree with PYTHIA 8 predictions (suppression) for high p_T-jets

Scope of looking at higher jet p_T

Results and Discussions

z^{ch}

Further investigation in PYTHIA 8 : absence of QGP medium

P. Das, A. Modak, **D.Banerjee**, et.al., arXiv:_2209.00972

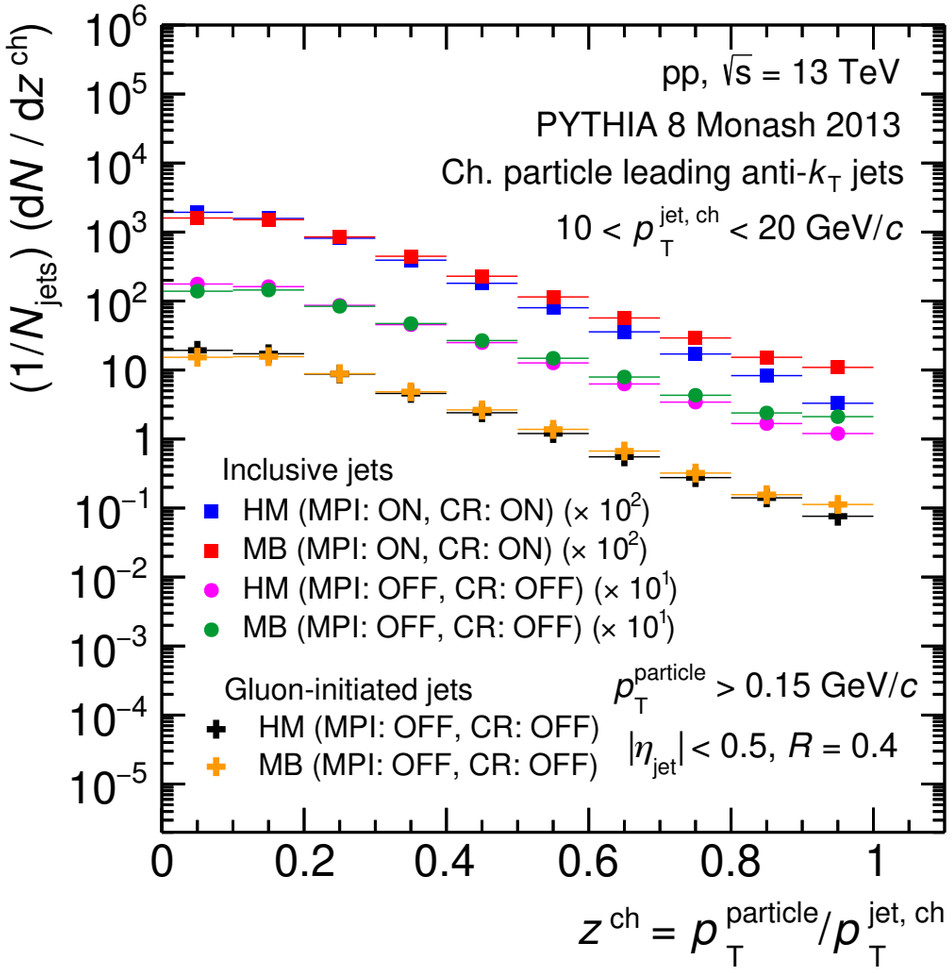

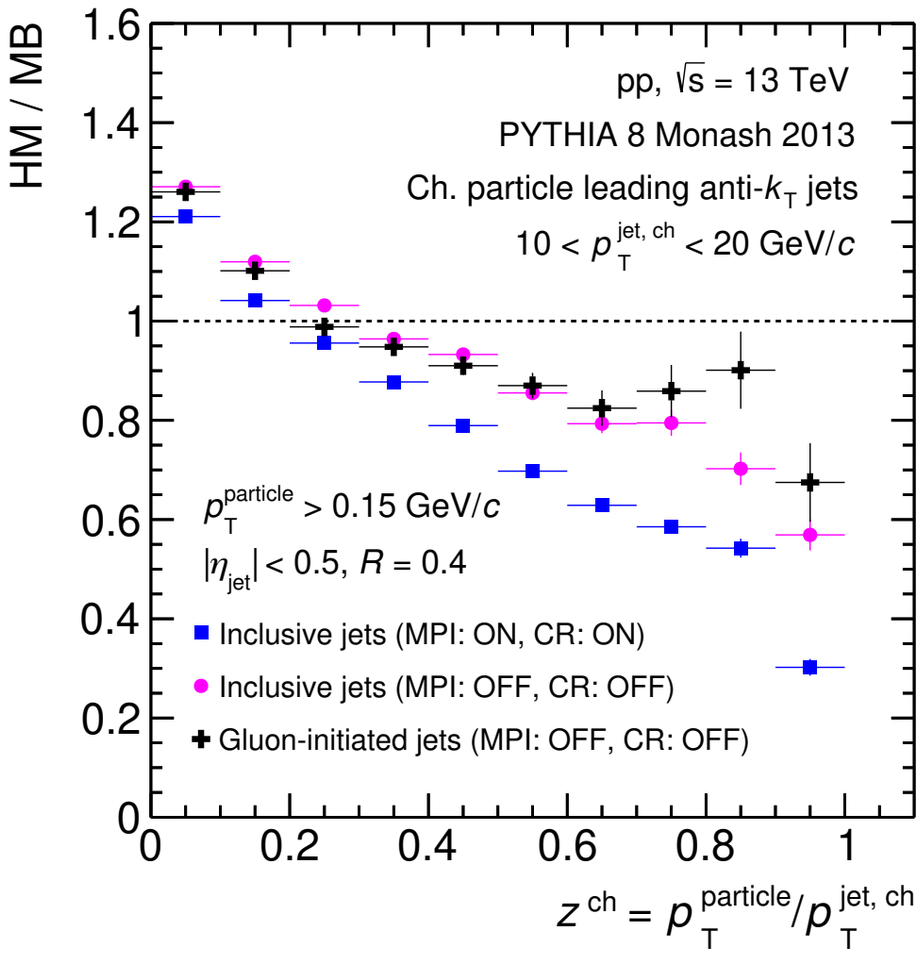

See Prottoy's talk in the afternoon session

Major contributions:

- ✓ Multiparton interactions (MPI) with color reconnection (CR) in PYTHIA 8
- ✓ Enhanced gluonic contributions in HM events

Results and Discussions

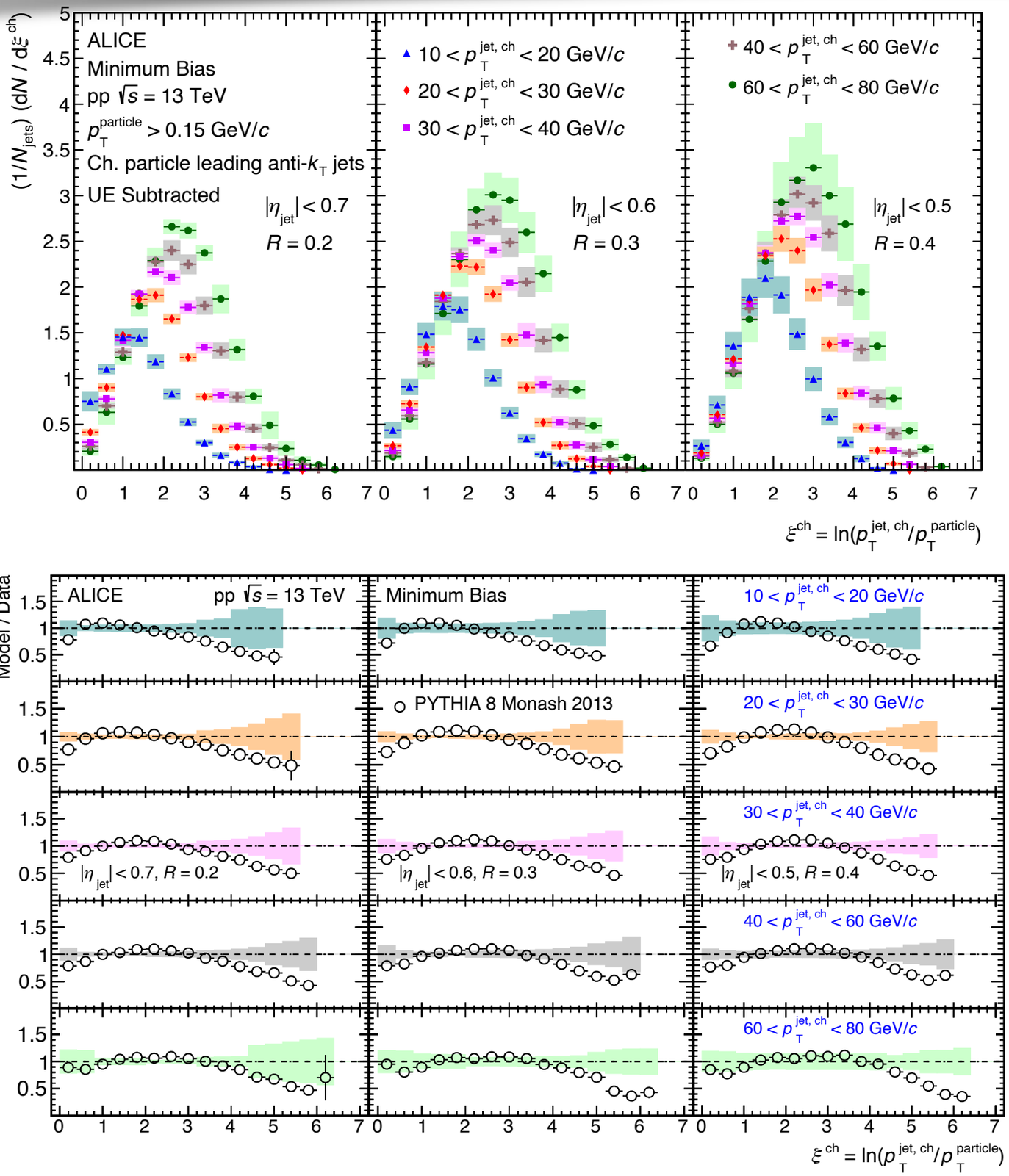

Jet fragmentation: jet p_T dependence

- Scaling with jet p_T: $\xi^{ch} < 2$
- Hump-backed plateau: suppression of low p_T particle production predicted by QCD coherence
- With increasing jet p_T and jet R, area of the distribution increases
- Complementing N_{ch} distributions

✓

MC predictions:

✓PYTHIA 8 qualitatively describes the data

Similar observations for HM events

Results and discussions

HM/MB (10-20 GeV/c)

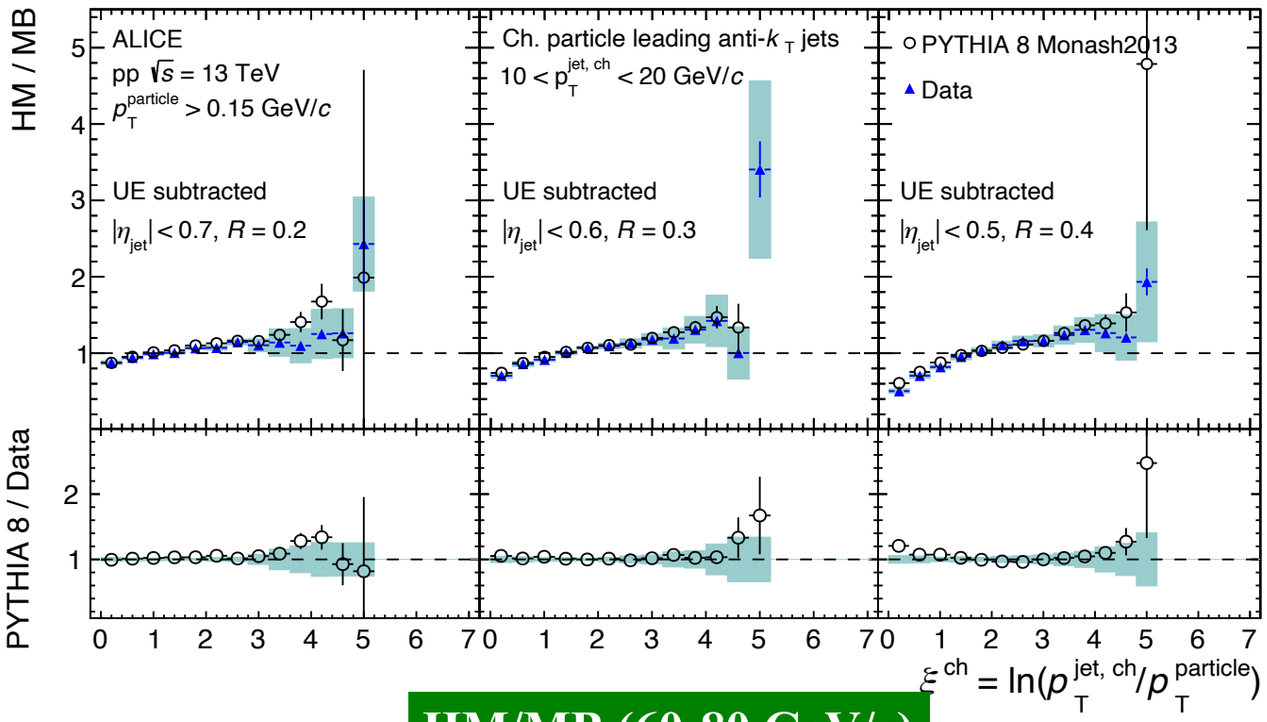

HM/MB (30-40 GeV/c)

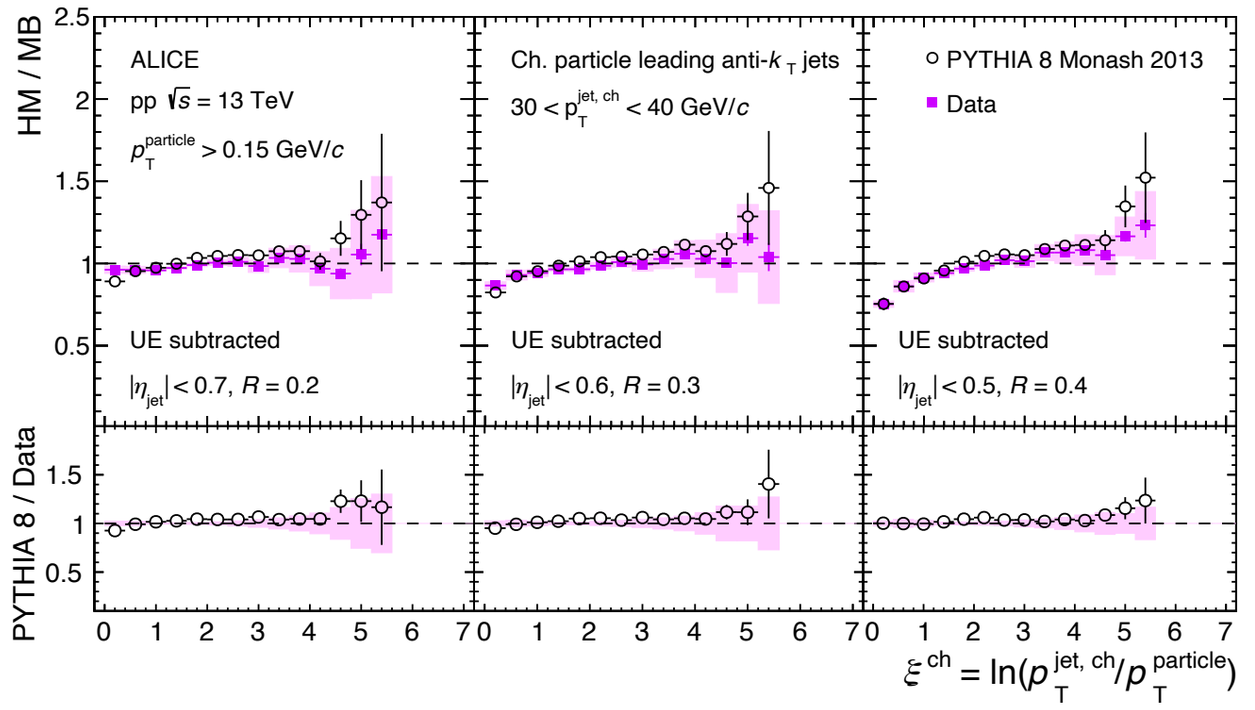

HM/MB (60-80 GeV/c)

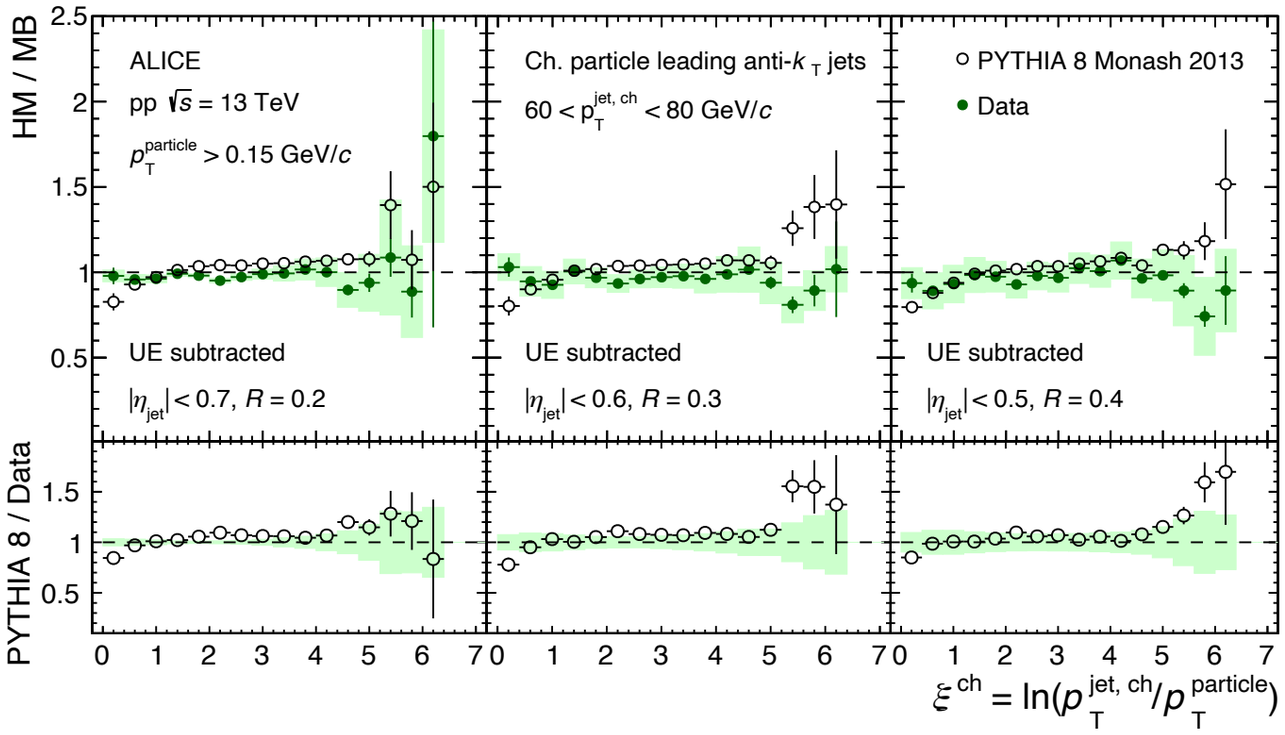

Modification in jet fragmentation!

PYTHIA 8 describes the data within systematic uncertainty

- Significant modification at low jet p_T (10-20 GeV/c)
- Dependence with jet p_T and jet R
- Modification reduces at high jet p_T (60-80 GeV/c)

Summary and Outlook

- ✓ First measurement of multiplicity-dependent charged-particle jet properties in pp collisions at 13 TeV
- ✓ Mean charged-particle multiplicity increases with increasing jet p_T and jet R for both HM and MB events
- ✓ Jet p_T independent scaling of jet fragmentation functions for wider jets in both HM and MB events
- ✓ A slight enhancement in $\langle N_{ch} \rangle$ is observed in HM compared to MB
- ✓ Significant modification of jet fragmentation in HM compared to MB
- ✓ PYTHIA 8 reproduces the modifications in HM compared to MB
- ✓ MPI with CR and enhanced gluonic contributions are playing major role

We observed jet modification in high-multiplicity pp collisions!

Shifting the question towards

How one can attribute the observed modification to different cases?

Jet quenching in mini-QGP, MPI with CR…?

Investigation of Jet modification in p-Pb collisions are coming….

Stay tuned!

Backup

Slide 3 and 4

Phase transition

In lattice-QCD calculations, the chiral susceptibility is the order parameter distinguishing the phases. It is defined as, χ (N_S , N_τ) = ($\partial^2 / \partial m^2_{ud}$)(T /V) log Z where Z is the partition function, m_{ud} is the mass of the light u, d quarks, N_S is the spatial extension, N_τ is euclidean time extension, and V the system volume in lattice-QCD. The smooth crossover was proved by showing that the temperature dependence of the peak and the width of the chiral susceptibility are independent of the system volume. For a typical first-order phase transition, the height of the susceptibility peak should have been proportional to the volume, and the width would vary inversely with volume. For a second-order transition, a singular behavior should have been observed with the volume of the system (V^α, α is a critical exponent).

Strangeness enhancement

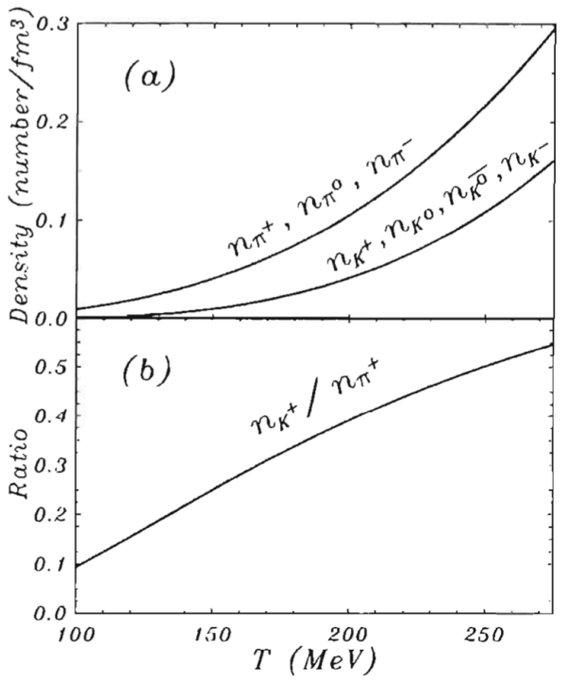

Fig. 18.1 (a) Pion and kaon densities as a function of hadron temperature T. (b) The ratio of K^+ density to π^+ density, as a function of temperature.

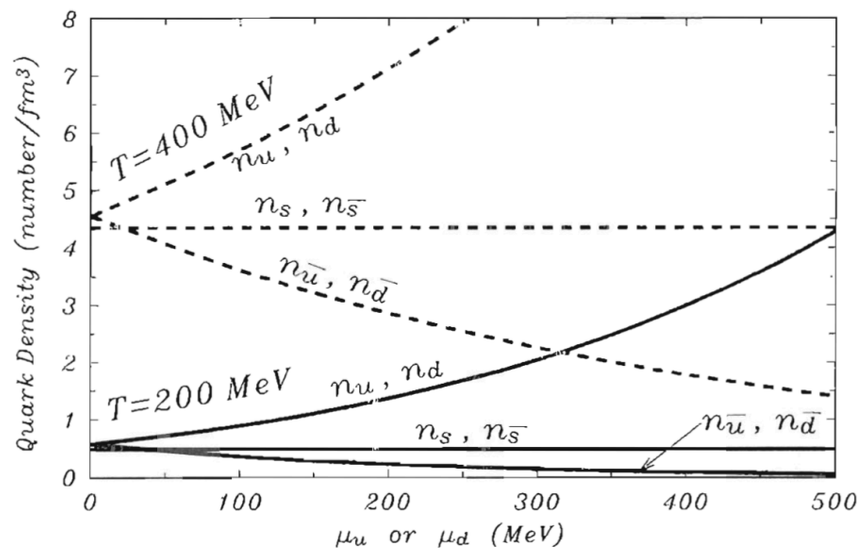

Fig. 18.2 Densities of various types of quarks and antiquarks as a function of the chemical potentials of the up or down quarks, μ_u or μ_d, at $T = 200$ and 400 MeV. The chemical potential μ_s of the strange quarks is constrained to be zero to give $n_s = n_{\bar{s}}$.

Hyperon				Anti-hyperon		
	Quarks	S	I		Quarks	S
Λ	uds	-1	0	$\overline{\Lambda}$	$\bar{u}\bar{d}\bar{s}$	1
Σ^+	uus	-1	1	$\overline{\Sigma}^+$	$\bar{u}\bar{u}\bar{s}$	1
Σ^0	uds	-1	1	$\overline{\Sigma}^0$	$\bar{u}\bar{d}\bar{s}$	1
Σ^-	dds	-1	1	$\overline{\Sigma}^-$	$\bar{d}\bar{d}\bar{s}$	1
Ξ^0	uss	-2	$\frac{1}{2}$	$\overline{\Xi}^0$	$\bar{u}\bar{s}\bar{s}$	2
Ξ^-	dss	-2	$\frac{1}{2}$	$\overline{\Xi}^-$	$\bar{d}\bar{s}\bar{s}$	2
Ω^-	sss	-3	0	$\overline{\Omega}^-$	$\bar{s}\bar{s}\bar{s}$	3

Consider the fate of an s quark and an $\bar{s}$ antiquark in a medium with nonzero chemical potential $\mu_{u,d}$. Because the densities of u and d are greater than the densities of $\bar{u}$ and $\bar{d}$, it is much more likely for the $\bar{s}$ antiquark to combine with a u or a d quark to form $K^+(u\bar{s})$ or $K^o(d\bar{s})$ than it is for the strange quark s to combine with a $\bar{u}$ or a $\bar{d}$ to form $\overline{K}^o(\bar{u}s)$ and $K^-(\bar{d}s)$. For the strange quark s, a more likely outcome is for it to combine with u and d quarks to form $\Lambda(uds)$, $\Sigma^+(uus)$, $\Sigma^o(uds)$, or $\Sigma^-(dds)$, instead of combining with $\bar{u}$ and $\bar{d}$ to produce $\overline{K}^o$ and K^-. Experimental measurements which can probe the numbers of s and $\bar{s}$ relative to the numbers of u, d, $\bar{u}$ and $\bar{d}$ can be used to find out the thermodynamical state of the quark-gluon plasma in the stopping region.

Near-side ridge

$$R(\Delta\eta, \Delta\phi) = \left\langle (\langle N \rangle - 1) \left(\frac{S_N(\Delta\eta, \Delta\phi)}{B_N(\Delta\eta, \Delta\phi)} - 1 \right) \right\rangle_{\text{bins}} \tag{4.1}$$

where S_N and B_N are the signal and random background distributions, defined in eqs. (4.2) and (4.3) respectively, $\Delta\eta (= \eta_1 - \eta_2)$ and $\Delta\phi (= \phi_1 - \phi_2)$ are the differences in pseudo-rapidity and azimuthal angle between the two particles, $\langle N \rangle$ is the number of tracks per event averaged over the multiplicity bin, and the final $R(\Delta\eta, \Delta\phi)$ is found by averaging over multiplicity bins. For simplicity in eq. (4.1) and the discussion in this section, N is used to represent the total number of offline reconstructed tracks per event. Note that the order in which the particles are considered has no significance. The quantities $\Delta\eta$ and $\Delta\phi$ are always taken to be positive and used to fill one quadrant of the $\Delta\eta, \Delta\phi$ histograms with the other three quadrants filled by reflection. Therefore, the resulting distributions are symmetric about $(\Delta\eta,\Delta\phi)=(0,0)$ by construction.

For each multiplicity bin, the signal distribution:

$$S_N(\Delta\eta, \Delta\phi) = \frac{1}{N(N-1)} \frac{d^2 N^{\text{signal}}}{d\Delta\eta d\Delta\phi} \tag{4.2}$$

was determined by counting all particle pairs within each event, using the weighting factor $N(N-1)$, then averaging over all events. This represents the charged two-particle pair density function normalized to unit integral. The background distribution:

$$B_N(\Delta\eta, \Delta\phi) = \frac{1}{N^2} \frac{d^2 N^{\text{mixed}}}{d\Delta\eta d\Delta\phi} \tag{4.3}$$

denotes the distribution of uncorrelated particle pairs representing a product of two single-particle distributions, also normalized to unit integral. This distribution was constructed by randomly selecting two different events within the same multiplicity bin and pairing every particle from one event with every particle in the other (in this case, the normalization factor $1/N^2$ corresponds to $1/N_1 N_2$ event-by-event). The pairs of events used to compute the background were also required to be within the same 0.5 cm wide bin in the vertex location along the beam.

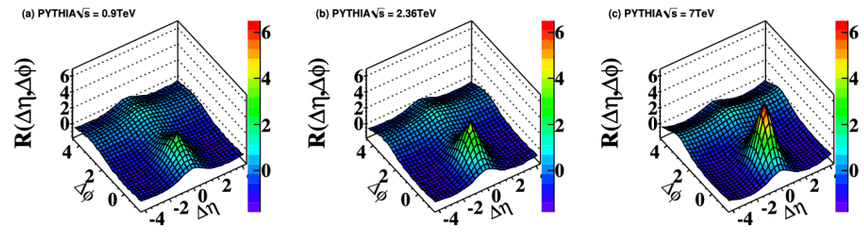

Figure 3. Two-particle correlation functions versus $\Delta\eta$ and $\Delta\phi$ in PYTHIA D6T tune at $\sqrt{s}$ = (a) 0.9, (b) 2.36, and (c) 7 TeV.

The novel structure in the high multiplicity *pp* data is reminiscent of correlations seen in relativistic heavy ion data. In the latter case, the observed long-range correlations are generally assumed to arise from various components of hydrodynamic flow of the produced medium [9, 36–39], from interactions between hard scattering processes and the medium, and from collective effects in the initial interaction of the nuclei.

However, new correlations can also start to emerge in the new energy regime probed here due to more elementary processes. For example, long range correlations are predicted also to occur in systems with a large number of fluctuating components, e.g. originating from additional color string connections. Such effects are presently not modeled in the MC generators.

ALICE detector

Sub-detectors: 18
Central-barrel detectors,
the forward detectors,
the trigger detectors,
and the muon spectrometers

The central part of ALICE is enclosed in the L3 solenoid, which has an internal length of 12.1 m and a radius of 5.75 m, B = 0.5T.

Event activity selection in pp collisions at $\sqrt{s}$ = 13 TeV

Online data triggers based on V0 detectors:

- Minimum-bias (MB) trigger → $L_{\text{Int}} \approx 32\ \text{nb}^{-1}$
- High-multiplicity (HM) trigger → $L_{\text{Int}} \approx 10^{4}\ \text{nb}^{-1}$

Offline event activity (EA) selection:

V0M = V0A + V0C → sum of signals

Characterization of EA in terms of V0M/⟨V0M⟩

⟨V0M⟩ - mean of MB distribution

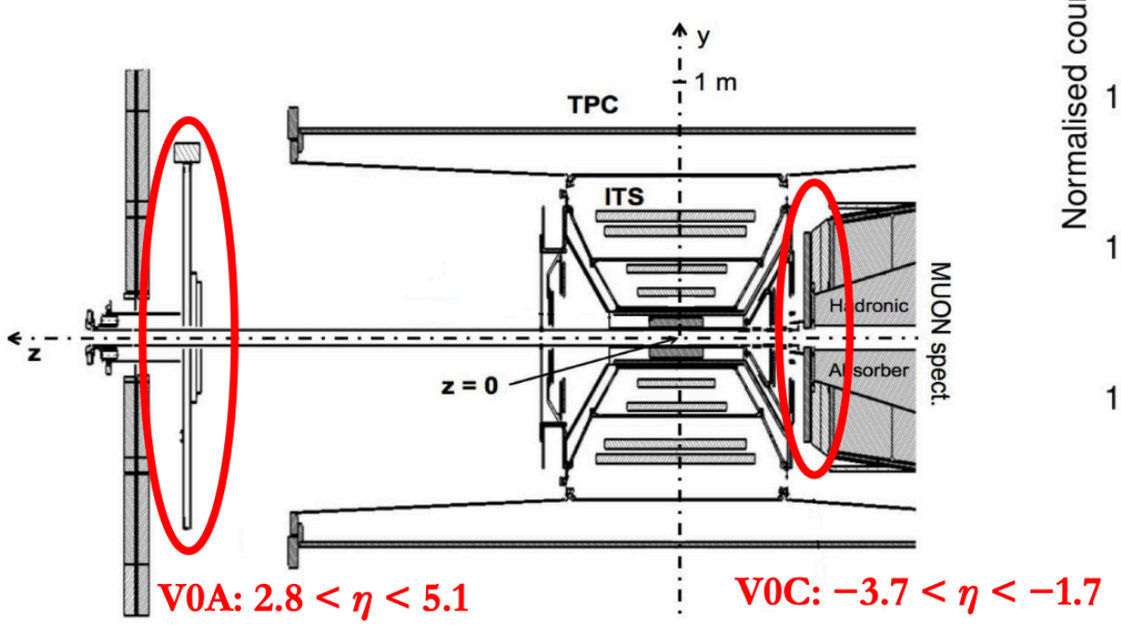

ALICE, Eur.Phys.J.C 82 (2022) 6, 514

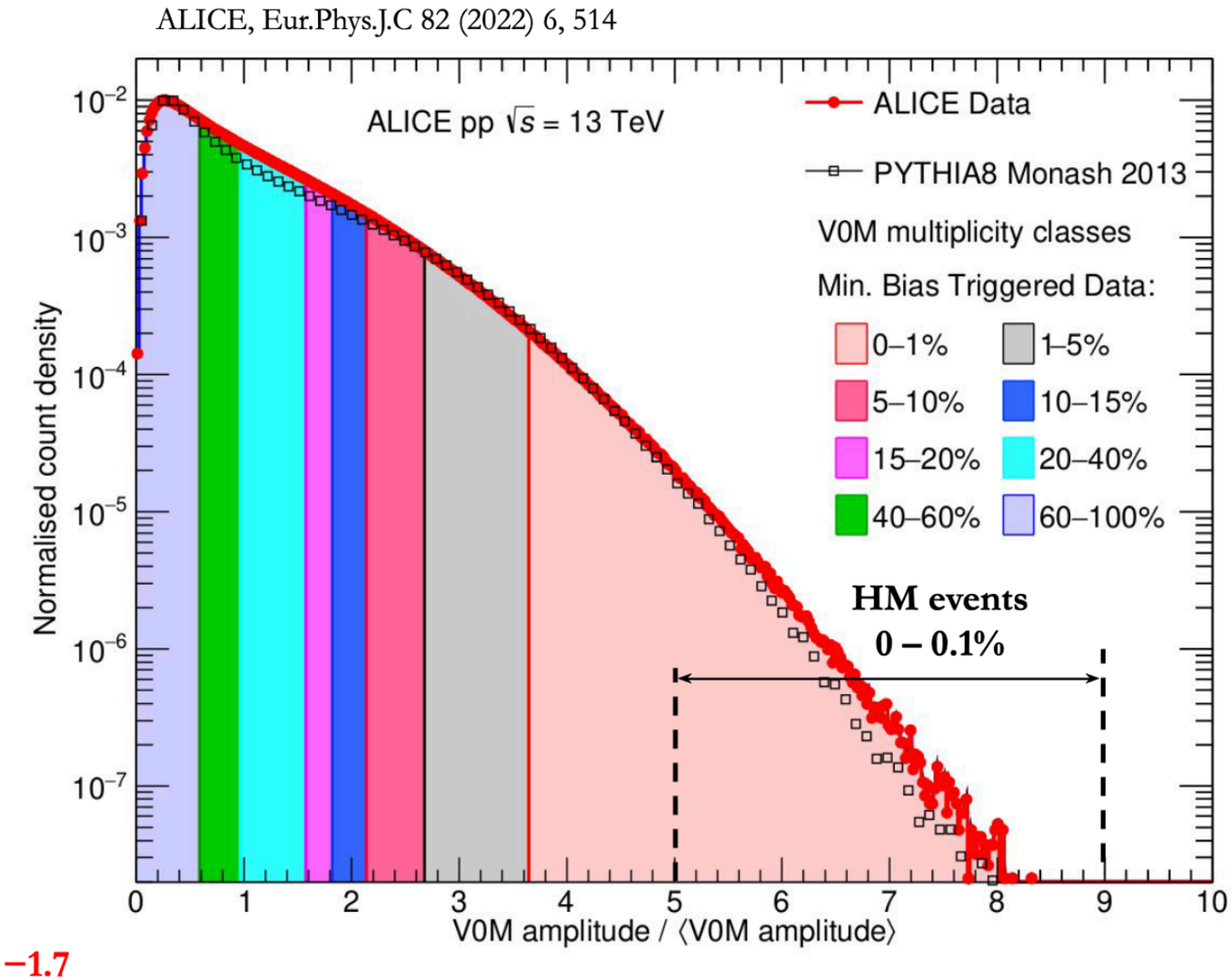

Slide 9

Vertex selection

4. Vertex distributions?

(a) What is the vertex distribution?

Ans: Vertex is the point where after collision all reconstructed tracks should meet. Event by event this point should meet somewhere but it varies and gives a distribution of the vertex position which is named by vertex distribution.

(b) From which point we measure vertex?

Ans: The reference point is the nominal interaction point where the collision is supposed to occur within the whole detector system. So all collisions should occur on that Geometrical or Nominal interaction point. All instrumentation can occur according to the nominal interaction point as a reference. Vertex distribution shows how the vertex varies from event to event, as we get one vertex point for one event.

(b) How do you determine vertex of an event?

Ans:

Tracking in the central barrel starts with the determination of the interaction vertex using the two innermost layers (SPD) of the ITS. It is found as a space point to which a maximum number of tracklets (lines defined by pairs of clusters, one cluster in each SPD layer) converge. In pp collisions, where interaction pileup is expected, the algorithm is repeated several times, discarding at each iteration those clusters which contributed to already-found vertices. By construction, the first vertex found has the largest number of contributing tracklets and is assumed to be the primary one. When a single convergence point is not found (particularly in low-multiplicity events) the algorithm performs a one-dimensional search of the maximum in the z-distribution of the points of closest approach (PCA) of tracklets to the nominal beam axis.

Steps:

- Clusterization step, in which the detector data are converted into "clusters" characterized by positions, signal amplitudes, signal times, etc., and their associated errors. The Clusterization is performed separately for each detector.
- The next step is to determine the preliminary interaction vertex using clusters in the first two ITS layers (SPD). Subsequently, track finding and fitting is performed in TPC and ITS using the Kalman filter technique.
- The found tracks are matched to the other central-barrel detectors and fitted. The final interaction vertex is determined using the reconstructed tracks.

- Once the tracks and the interaction vertex have been found in the course of event reconstruction, a search for photon conversions and secondary vertices from particle decays is performed

(c) Why do we take vertex cut within 10cm?

Ans: To minimize dependencies of the TPC acceptance on the vertex position.

Jet selection

Jet finding algorithms:

- Experimentally jets can be defined as a set of collimated particles which are clustered as a single entity as they are subjected to certain algorithms known as jet finding algorithms.
- Jet algorithms are nothing but a set of rules advocated in order to make groups of particles together (each group is entitled as a single 'jet') and can have one or more parameters.
- Two important types of jet algorithms are:
  (a) Cone algorithms
  (b) Sequential recombination algorithm

- We have used anti-k_T algorithm for jet finding ,which is a sequential recombination algorithm.

Anti-k_T Algorithms:

(i) For each pair of particles the distance

$$d_{ij} = min(p_{ti}^{-2}, p_{ti}^{-2})\frac{\Delta R_{ij}^2}{R^2} \quad (1)$$

is measured where

$$\Delta R_{ij} = \sqrt{(\eta_i - \eta_j)^2 + (\phi_i - \phi_j)^2} \quad (2)$$

is the distance between two particles (i-th and j-th) in (η - ϕ) plane, R = jet radius and p_{ti} and p_{tj} are the transverse momentum of the i-th and j-th particles respectively.

(ii) Additionally, particle-beam distance for each particle, given by

$$d_{iB} = p_{ti}^{-2} \quad (3)$$

is also measured.

(iii) The minimum of d_{iB} with d_{ij} is found out.

(iv) If it is a d_{ij}, i-th and j-th particles are recombined into a single new object whose momentum is (p_{ti} + p_{tj}) and it is often called a "pseudojet", since it is neither a particle nor yet a full jet.

(v) Otherwise, if the minimum is a d_{iB}, i-th particle is considered to be part of "beam" jet and it is removed from the list.

Slide 10

Unfolding performance

The default number of iteration is chosen as the one that minimizes the total uncertainty.

Summed Error = $\sqrt{(SE_{Iter})^2 + (SE_{Prior})^2 + (SE_{Stat})^2}$

$(\mathrm{SE_{Iter.}})^2 = \sum_i^{N_{bins}} \left(\frac{1}{2} \sqrt{(Obs_i^{it+1} - Obs_i^{it})^2 + (Obs_i^{it-1} - Obs_i^{it})^2} \right)^2$

$(\mathrm{SE_{Prior}})^2 = \sum_i^{N_{bins}} \left(Obs_i^{Modified} - Obs_i^{Default} \right)^2$

$(\mathrm{SE_{Stat.}})^2 = \sum_i^{N_{bins}} \left(Err\_Obs_i^{Default} \right)^2$

5.1 Unfolding errors with the Bayes method

As shown on the left-hand side of Fig. 5, the uncertainties calculated by propagation of errors in the Bayes method were found to be significantly underestimated compared to those given by the toy MC. This was found to be due to an omission in the original method outlined by D'Agostini ([2] section 4).

The Bayes method gives the unfolded distribution ('estimated causes'), $\hat{n}(\mathrm{C}_i)$, as the result of applying the unfolding matrix, M_{ij}, to the measurements ('effects'), $n(\mathrm{E}_j)$:

$$\hat{n}(\mathrm{C}_i) = \sum_{j=1}^{n_\mathrm{E}} M_{ij} n(\mathrm{E}_j) \quad \text{where} \quad M_{ij} = \frac{P(\mathrm{E}_j|\mathrm{C}_i) n_0(\mathrm{C}_i)}{\epsilon_i f_j} \tag{2}$$

$P(\mathrm{E}_j|\mathrm{C}_i)$ is the response matrix, $\epsilon_i \equiv \sum_{j=1}^{n_\mathrm{E}} P(\mathrm{E}_j|\mathrm{C}_i)$ are efficiencies, and $f_j \equiv \sum_{l=1}^{n_\mathrm{C}} P(\mathrm{E}_j|\mathrm{C}_l) n_0(C_l)$ is the folded prior distribution, $n_0(C_l)$ — initially arbitrary (eg. flat or MC model), but updated on subsequent iterations.

Minimum bias

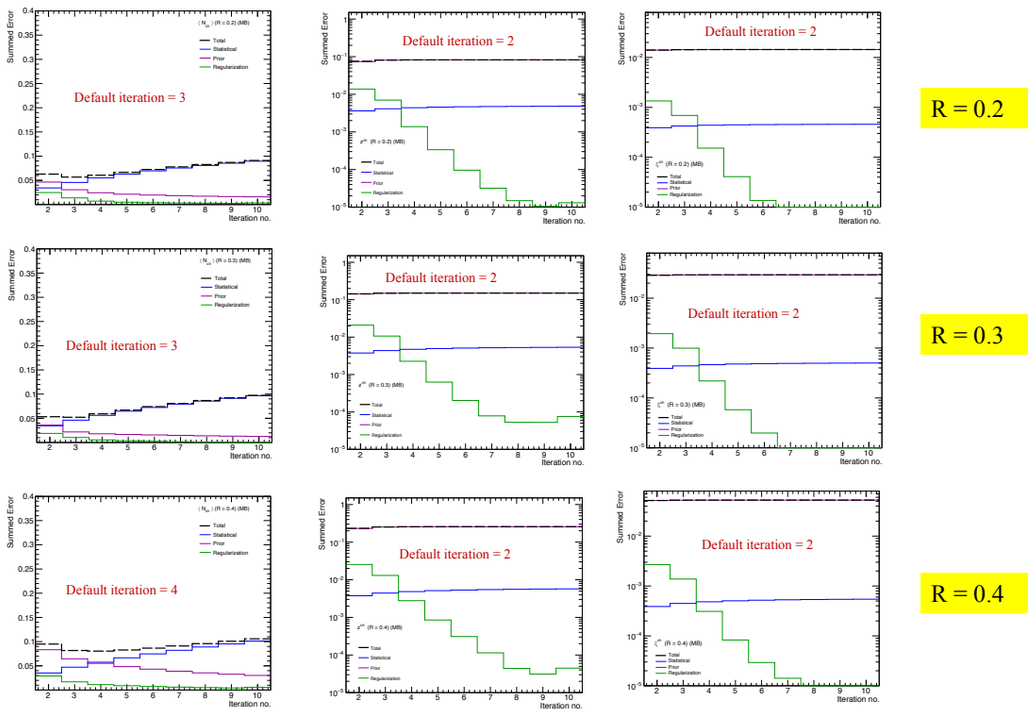

R = 0.2

R = 0.3

R = 0.4

High multiplicity

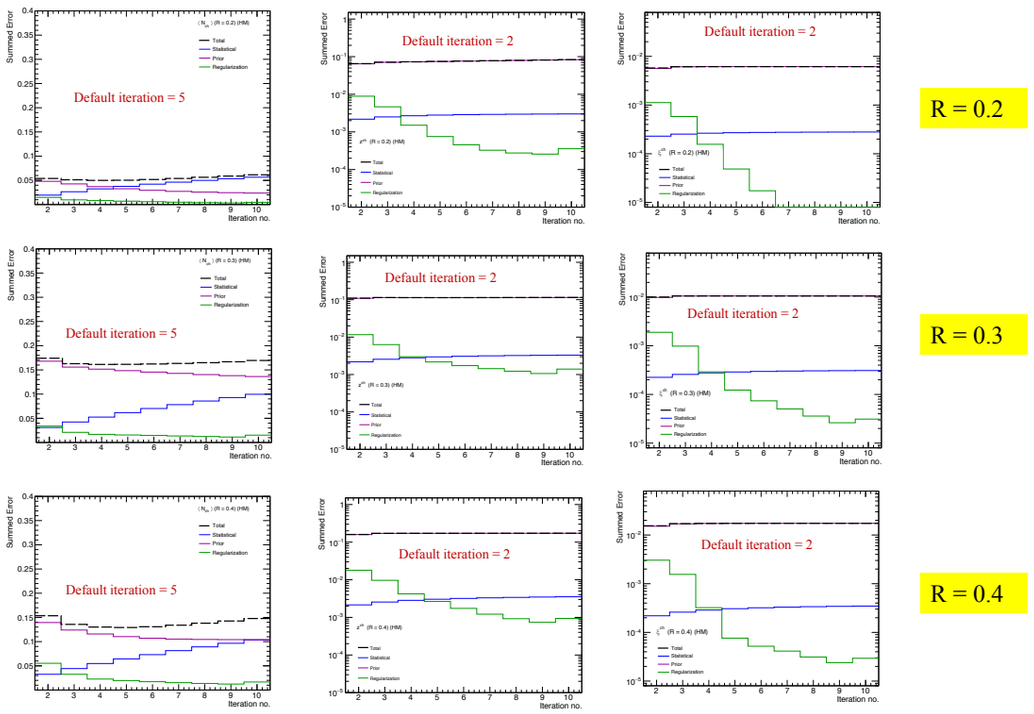

R = 0.2

R = 0.3

R = 0.4

Slide 10

Unfolding performance

2D Projection of response matrices

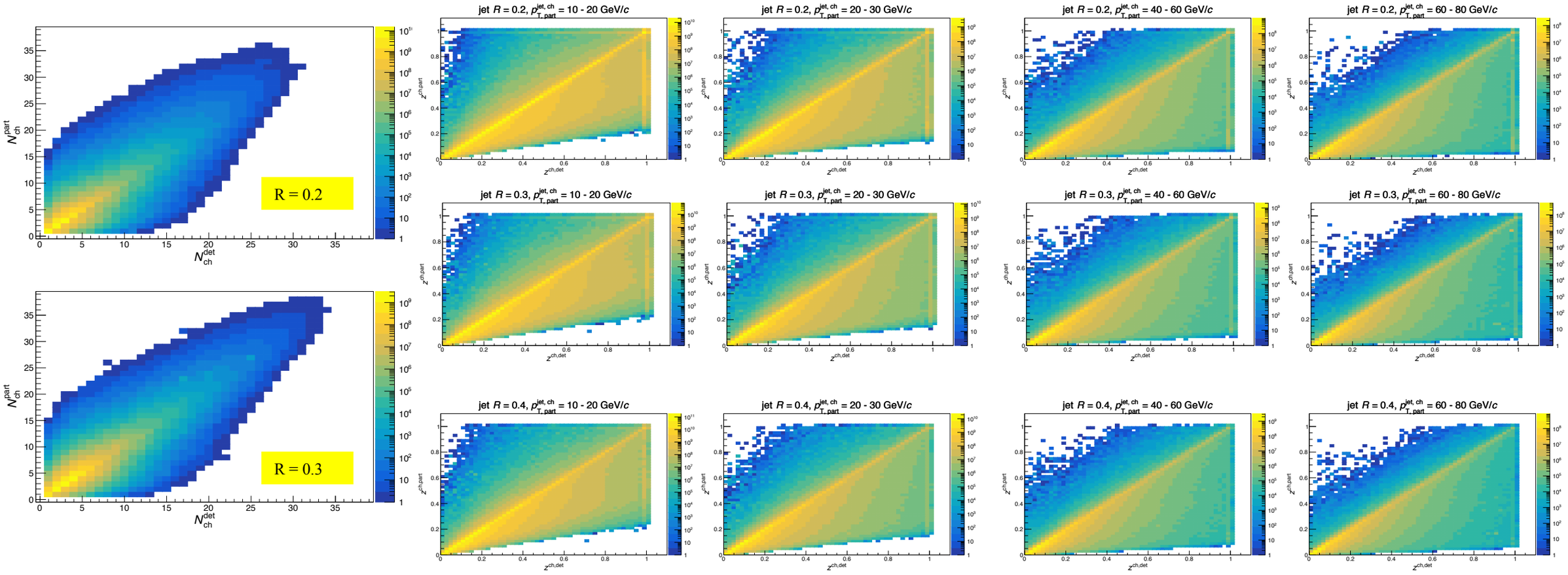

For ξ^{ch} see section 7.4 of AN (v5): https://alice-notes.web.cern.ch/node/1303

Unfolding closure

MB results

Statistical Closure test

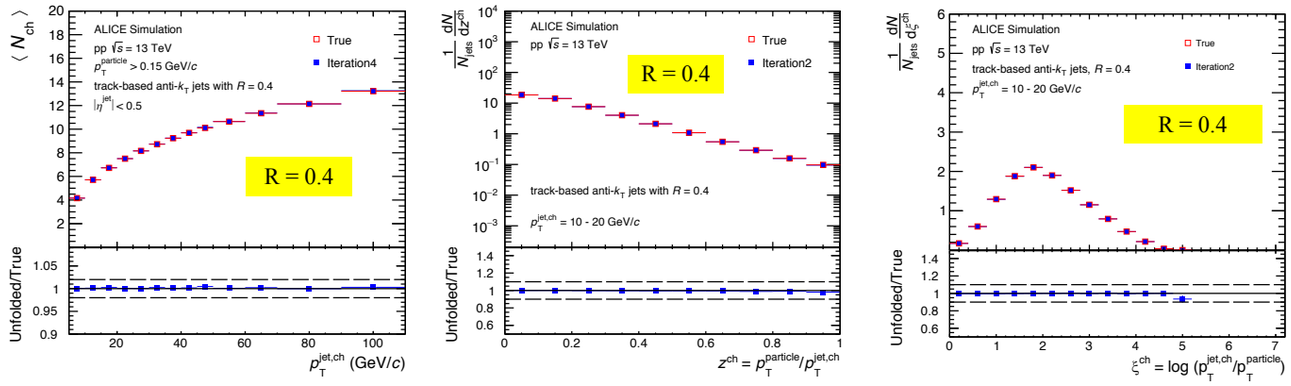

- Unfolded results are in good agreement with true distributions

<N_{ch}>: Jet radius (R = 0.2 and 0.3)
z^{ch} : Jet p_T = 10-20, 30-40, 40-60 and 60-80 GeV/c
ξ^{ch} : Jet p_T = 10-20, 30-40, 40-60 and 60-80 GeV/c

See backup slides

MB results

Shape Closure test

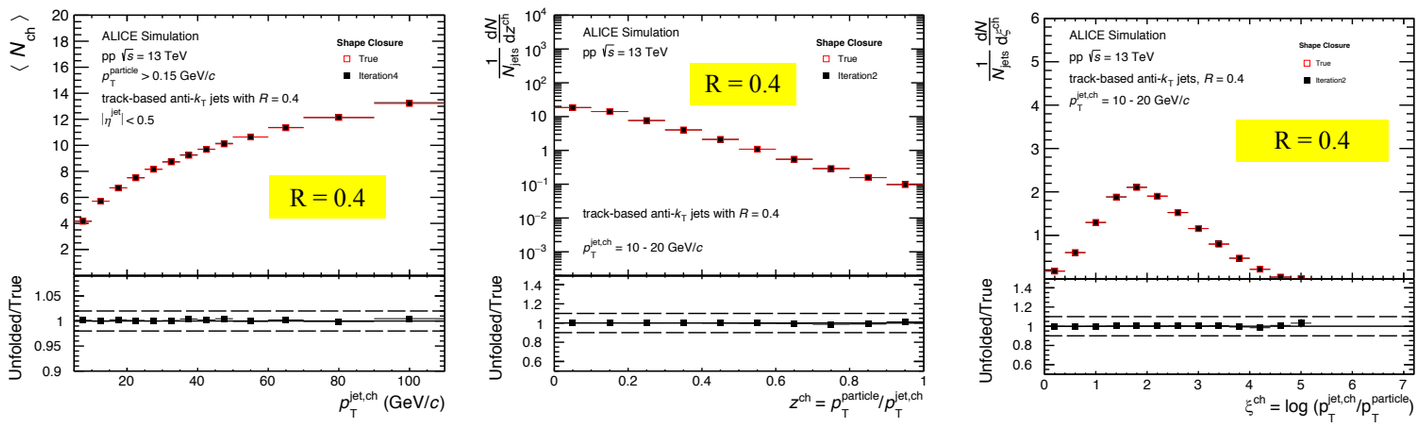

- Unfolded results are in good agreement with true distributions

<N_{ch}>: Jet radius (R = 0.2 and 0.3)
z^{ch} : Jet p_T = 10-20, 30-40, 40-60 and 60-80 GeV/c
ξ^{ch} : Jet p_T = 10-20, 30-40, 40-60 and 60-80 GeV/c

See backup slides

Systematic uncertainty

Systematic uncertainty

MB: R=0.4

HM: R=0.4

$\langle N_{ch} \rangle$

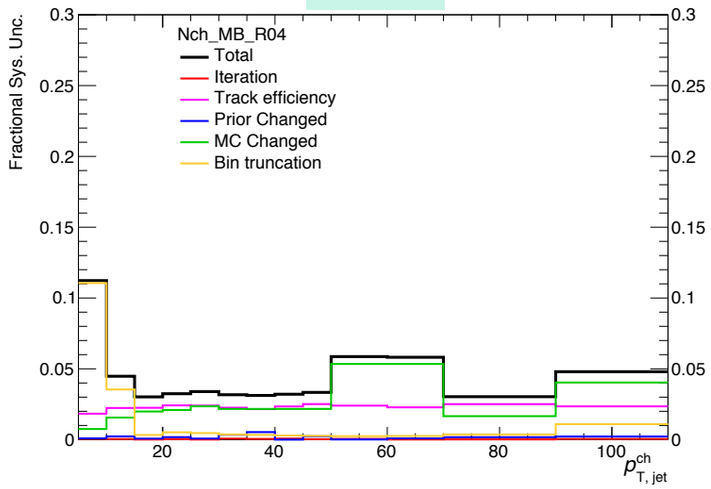

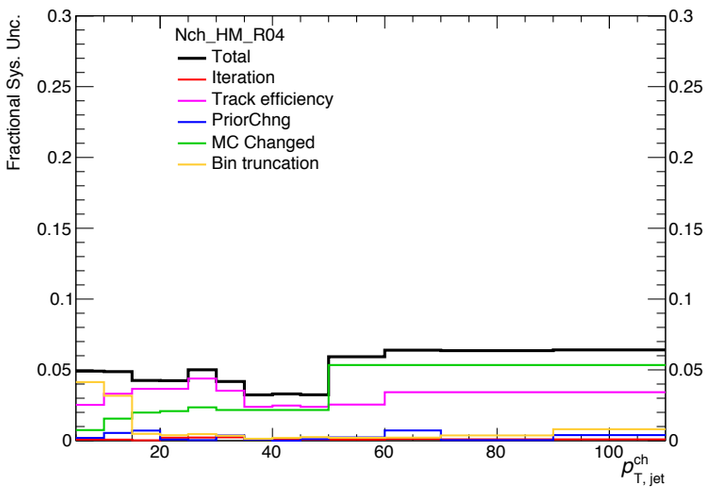

z^{ch} (Jet p_T = 10-20 GeV/c)

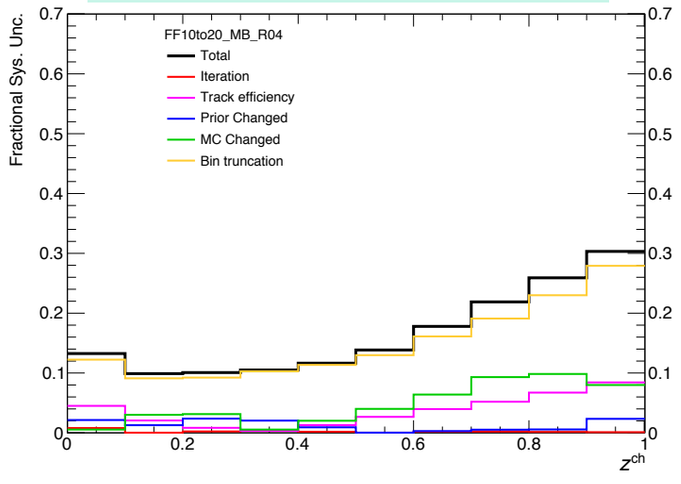

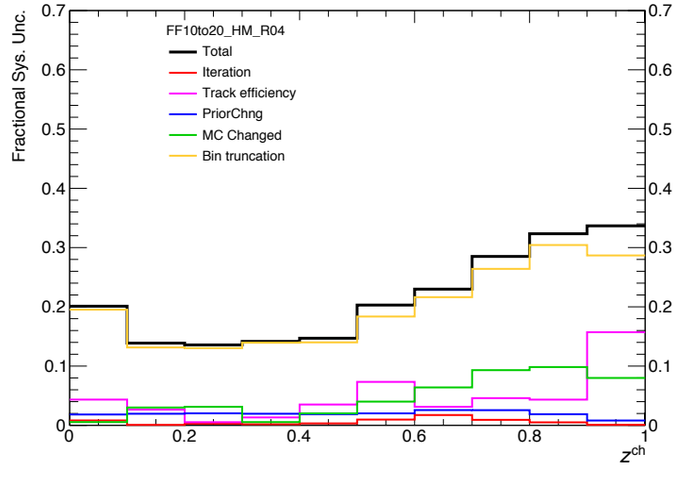

ξ^{ch} (Jet p_T = 10-20 GeV/c)

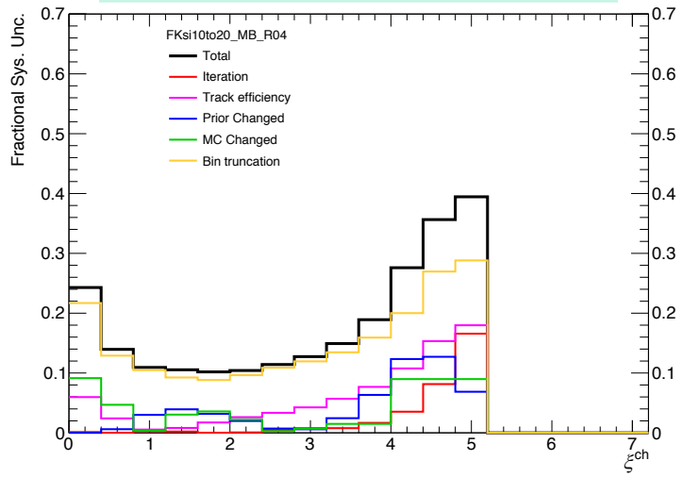

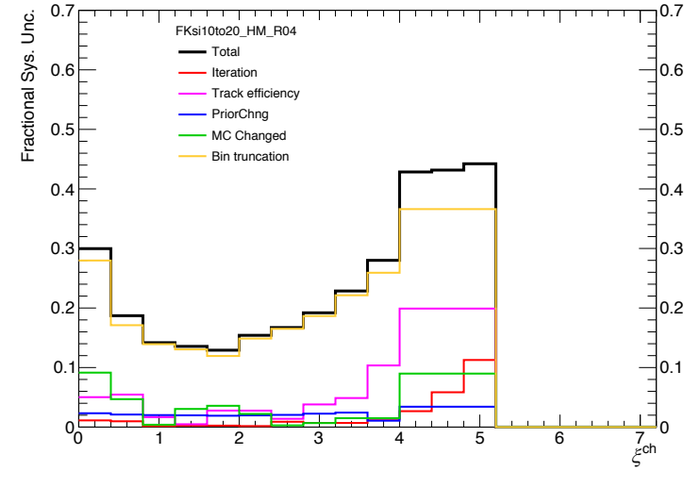

$\langle N_{ch} \rangle$: Jet radius (R = 0.2 and 0.3)
z^{ch} : Jet p_T = 10-20, 30-40, 40-60 and 60-80 GeV/c
ξ^{ch} : Jet p_T = 10-20, 30-40, 40-60 and 60-80 GeV/c

MPI is a natural consequence of the composite structure of the colliding hadrons, leading to several parton-parton interactions occurring in one hadron-hadron collision (the schematic is shown in Fig. 1) and is implemented in PYTHIA 8 through a single unified framework [66] that incorporates both soft and hard QCD MPI processes [67].

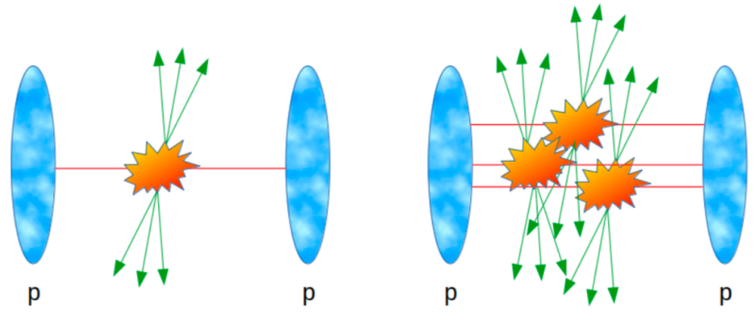

Figure 1: Single hard scattering (left) and multiple hard scatterings, i.e., MPI (right), occurring in a single proton-proton collision.

The implementation of the color reconnection mechanism in PYTHIA 8 is schematically illustrated in Fig. 2. The connection between the outgoing partons and the beam remnants through color strings in case of a single hard scattering is shown in Fig. 2a. A second hard scattering (Fig. 2b) can be naively expected to give rise to two new strings connected to the beam remnants. This would result in a proportional increase in multiplicity; however, to successfully fit the data (see Ref. [68] and references therein) it is instead assumed that the partons are color reconnected so that the total string length gets minimized (Fig. 2c).

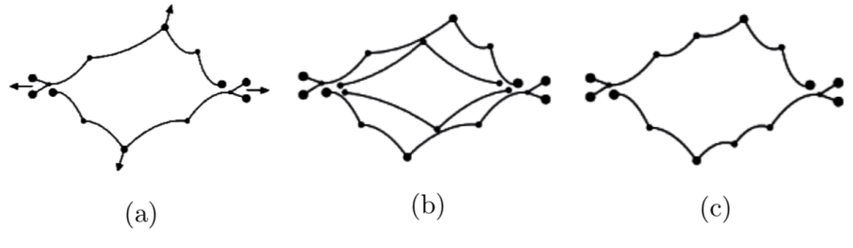

Figure 2: Illustration of the color reconnection mechanism in PYTHIA 8 (image directly extracted from Ref. [68]). (a) The outgoing gluons are color connected to the projectile and target beam remnants. (b) A second hard scattering with two new strings connected to the beam remnants. (c) Color reconnected partons minimizing the total string length.

MPIs occurring in a hadronic collision lead to the creation of an environment having several high-momentum partons along with the soft ones in a small region (the overlap area of the colliding hadrons), leading to high multiplicity events. The evolution of the scattered outgoing partons to final-state collimated hadrons (jets) via fragmentation and hadronization in such an environment is expected to be different compared to the situation with no MPI (only one hard scattering per hadronic collision), which could affect the differential jet shape properties. The fragmentation of independent hard scatterings (MPIs) becomes correlated due to the color reconnection mechanism [39] described earlier and is, therefore, expected to further modify the differential shape jet properties.

High-multiplicity (HM)

Results and discussions

z^{ch}

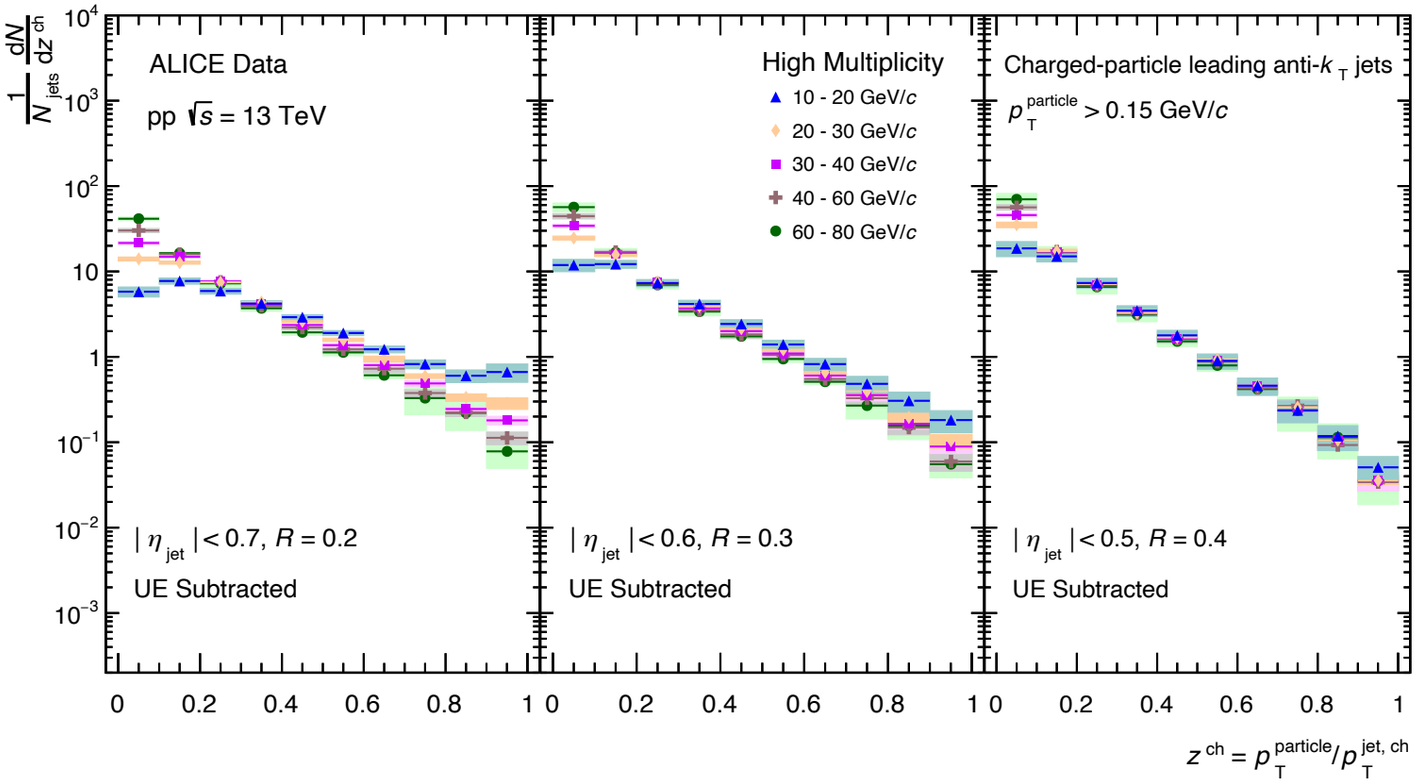

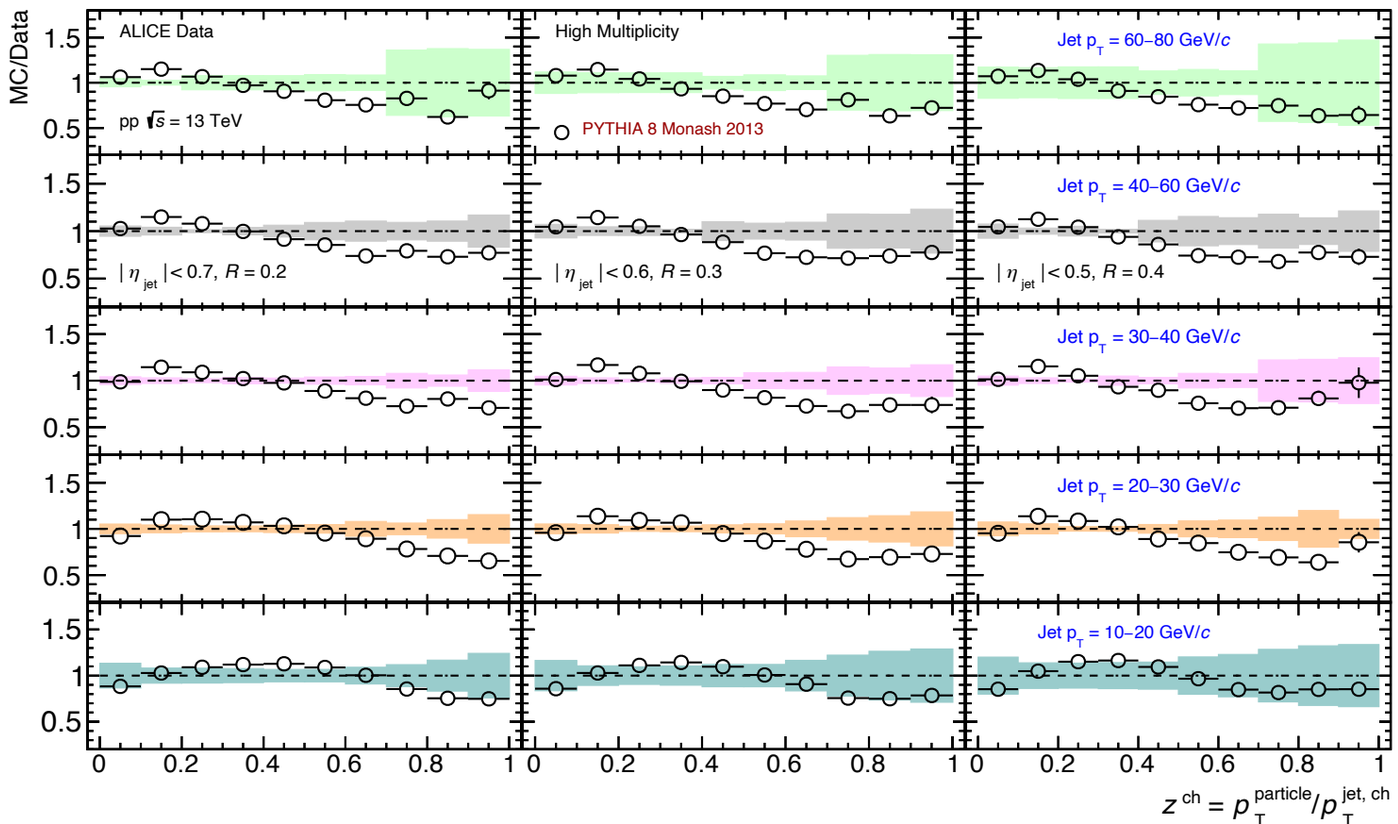

Jet fragmentation: jet p_T dependence

✓Scaling with jet p_T: Indication of jet p_T independent jet fragmentation for wider jets

MC predictions:

✓PYTHIA 8 describes the data within systematic uncertainty for lower and higher jet p_T ranges

✓PYTHIA 8 underestimate the data for intermediate z_{ch} values for intermediate jet p_T ranges

High-multiplicity (HM)

Results and discussions

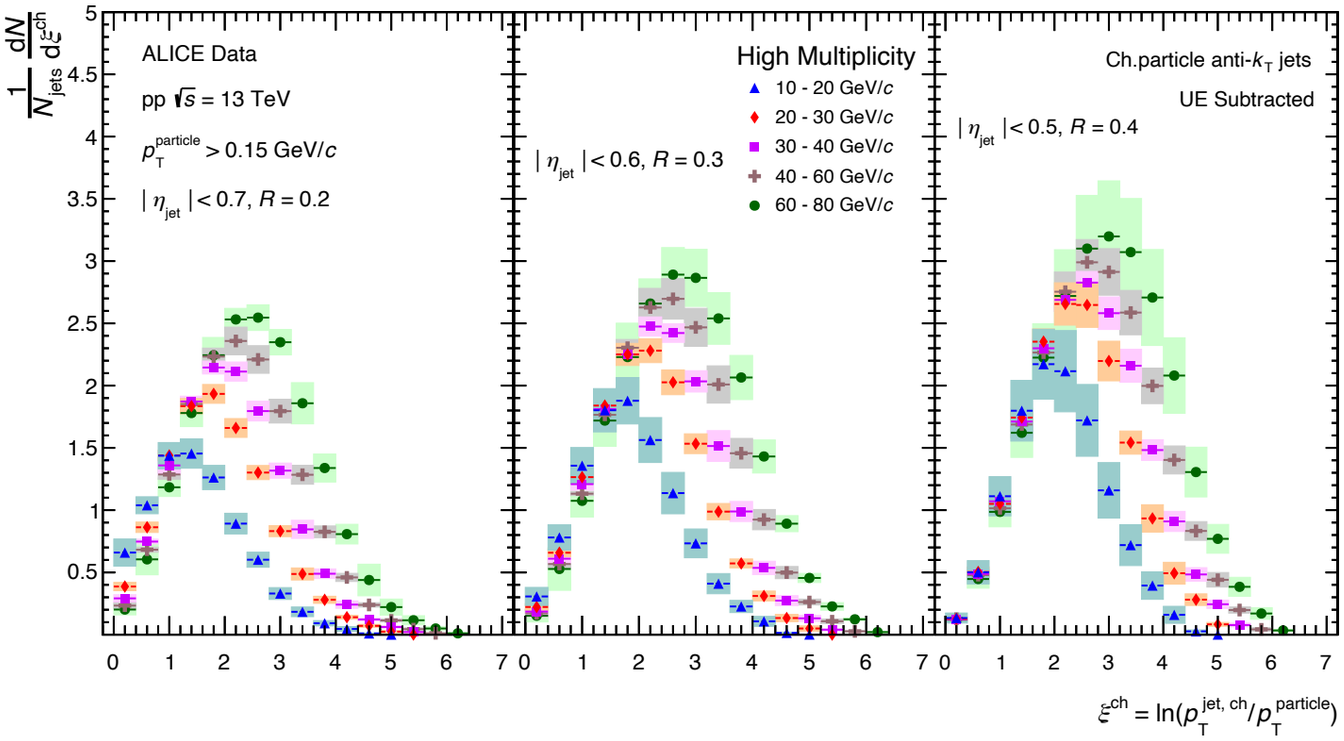

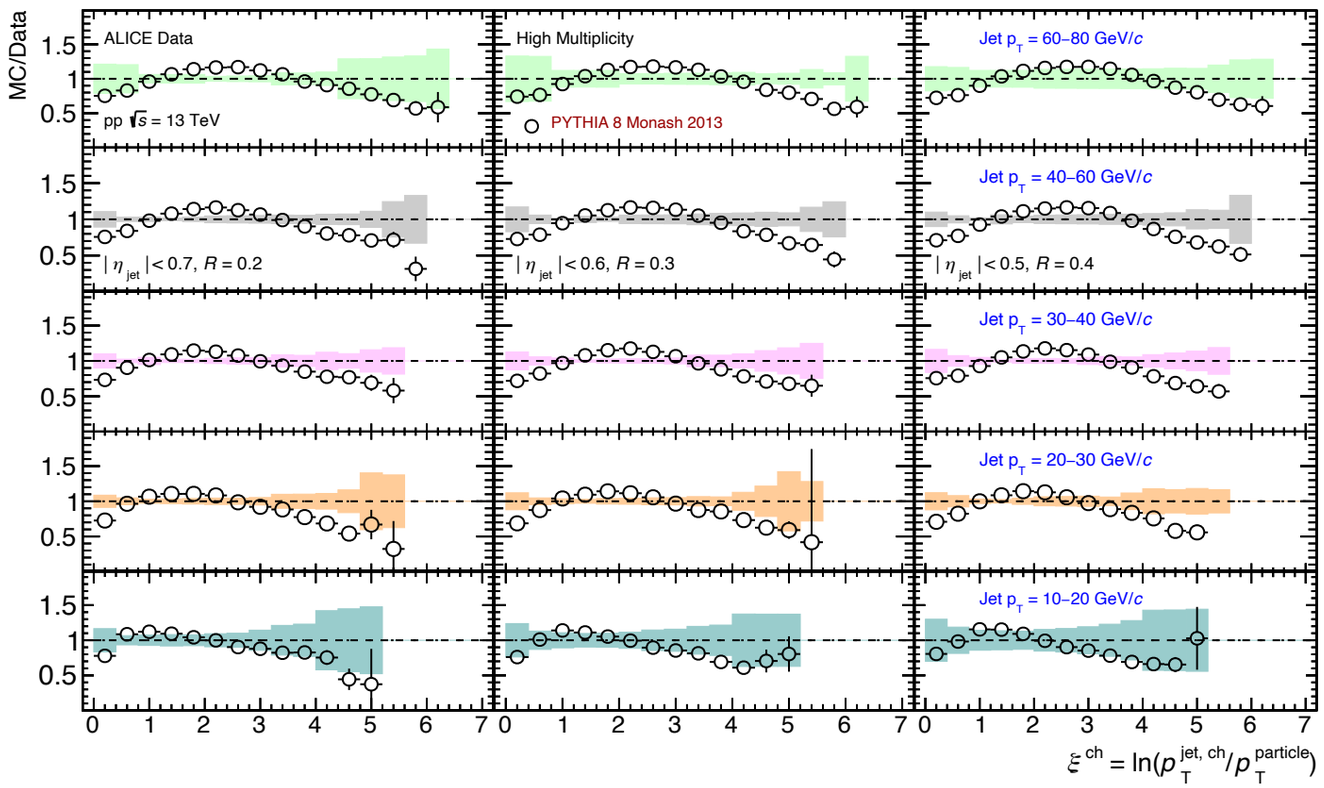

Jet fragmentation: jet p_T dependence

- Scaling with jet p_T: $\xi^{ch} < 2$
- Hump-backed plateau: suppression of low p_T particle production predicted by QCD coherence
- With increasing jet p_T and jet R, area of the distribution increases
- Complementing N_{ch} distributions

✓

MC predictions:

✓PYTHIA 8 qualitatively describes the data

PYTHIA 8 and EPOS LHC

PYTHIA 8 Monash 2013: The PYTHIA 8 event generator is a standard tool for the generation of high energy physics collisions dominantly based on 2 → 2 hard scattering processes. In pp interactions, the total hadronic cross section is obtained from the parameterization of Donnachie and Landshoff. The diffractive components of inelastic cross section are described by Schuler-Sjostrand model. Multiparton interactions (MPI) are described by an impact-parameter dependent approach where protons are considered as extended objects and therefore, collisions may vary from central to peripheral. More central means the bigger overlap between the colliding cloud of partons which leads to the large number of average MPIs per collision and thereby the number of produced particles is increased. MPI are also relevant to describe the modelling of soft underlying event (UE) in PYTHIA 8. An MPI-based model is implemented in PYTHIA 8 to introduce beam-remnants and color reconnection wherein all the gluons of a lower-pT interactions are merged with the color-flow dipoles of a higher-pT one, in such a way as to minimise the total string length. It has been shown that the color reconnection plays an important role to describe the scale of charged-particle pseudorapidity density as a function of multiplicity in pp collisions. The description of hadronisation mechanisms is based on the Lund string fragmentation framework. In Monash tune of PYTHIA 8, the parameters relevant for initial-state radiation and MPI are tuned by using the minimum-bias, Drell-Yan, and underlying event data from the Tevatron, SPS and LHC.

EPOS LHC: EPOS is a parton based MC model with flux tube initial condition for hadron-hadron collisions. It can also be used for heavy-ion collisions as well as cosmic ray air shower simulations. EPOS uses parton based Gribov Regge theory for describing soft interactions. EPOS LHC is the updated version of EPOS tuned to LHC data. In this tune, the modelling of radial flow has been modified via a different parametrization for a small volume with high density of thermalized matter (core) reached in pp interactions compared to the large volume produced in heavy-ion collisions.

Pythia 8 vs EPOS

1) Based on Leading order QCD => EPOS is based on Gribov-Regge Theory

2) pp collision can be represented by a plethora of processes like elastic and diffractive (described using Pomerons), soft and hard QCD processes etc. => In EPOS, elementary interactions between the constituent partons of nucleons proceed via exchanges of parameterised objects called Pomerons which have the quantum numbers of the vacuum.

3) Implements parton showers (Initial State Radiation, ISR, and Final State Radiation, FSR) => Not there in EPOS

4) Considers the phenomena such MPI, CR => CR most probably is not there in EPOS. In EPOS, multiple scattering occurs via multi-Pomeron exchanges

5) For hadronization, Pythia uses Lund String Fragmentation model. => In EPOS, hadronization is treated in a different way (core-corona approach). EPOS is a core-corona model. The core represents a region with a high density of string segments that is larger than some critical density for which the hadronization is treated collectively and the corona is the region with a lower density of string segments for which the hadronization is treated non-collectively. The strings from the core region form clusters which expand collectively. This expansion has two components, namely radial and longitudinal flow.

Multiplicity dependence of charged-particle intra-jet properties in pp collisions at 13 TeV

Paper Committee: **D. Banerjee (chair)**, P. Das, and S. K. Prasad
ALICE Collaboration,
Accepted in *European Physical Journal C,* arXiv: 2311.13322 [hep-ex]

Systematic uncertainty

Tracking inefficiency:

Detector-level tracks are randomly discarded by 3% before jet finding

Choice of different event generator [MC dependence]

PYTHIA 8 is used as default and EPOS LHC is used for systematic uncertainty

Choice of different regularisation parameter

Number of iteration is changed by +/- 1 from the default one

Change of the prior distributions

Response matrix is reweighted with the factor taken from the ratio between data and rec-level MC

Bin truncation

The lower and upper bounds of jet p_T of detector level jets are varied by +5 and -20 respectively

UE estimation method

Perpendicular cone method is used as default and random cone method is used as variation

In each case:

A modified response matrix is rebuilt with the variation and used to unfold the raw data

$$Systematic\ uncertainty = \frac{Modified - default}{default}$$

Total systematic uncertainty: quadrature sum of individual sources

Importance of jet study: HI collisions

Jets in the QGP:

- Jets propagate through the expanding and cooling QGP
- Jet shower itself evolves with QGP
- Jet constituents interact with the colour-charged constituents of the QGP
- Modification of jet shower: ***jet quenching***

One of the important probe of QGP medium

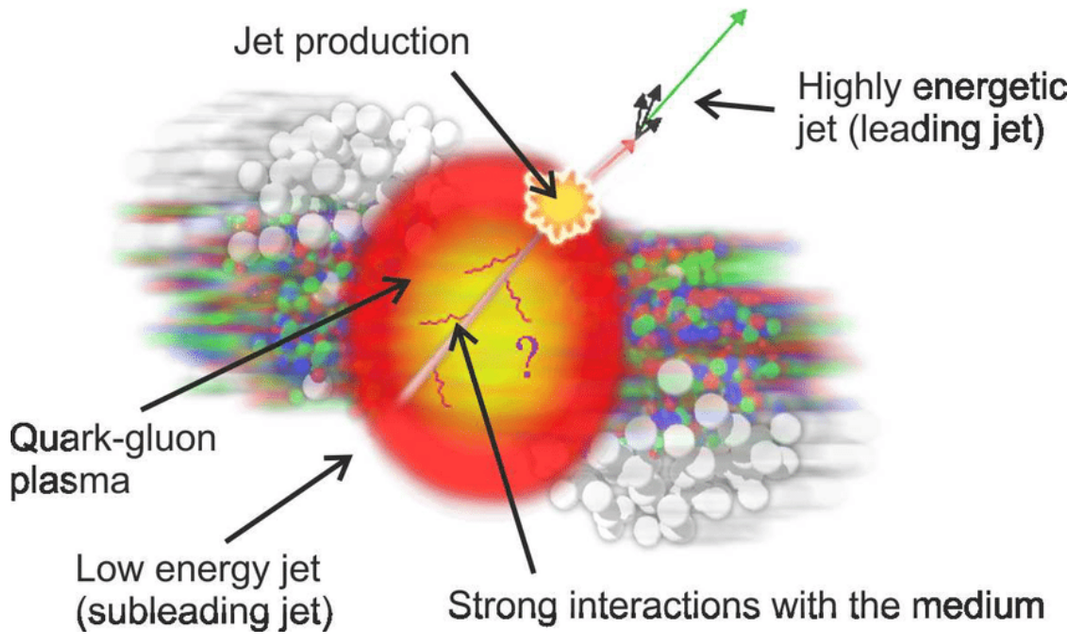

Jets in heavy-ion (AA) collisions [2]

[2] https://newscenter.lbl.gov/2010/01/14/jet/

Experimental observation of jet quenching:

- Medium-induced energy loss, observed through inclusive jet yield suppression in heavy-ion collisions compared to binary-scaled pp collisions; jet nuclear modification factor R_{AA}
- Medium-induced modification of the distribution of jet constituents, observed through the radial energy profile, jet substructure, and fragmentation functions

Theoretical calculation of jet quenching: jet transport coefficient